Geoderma 429 (2023) 116226

Contents lists available at ScienceDirect

Geoderma

journal homepage: www.elsevier.com/locate/geoderma

Process sequence of soil aggregate formation disentangled through multi-isotope labelling

Wulf Amelung [a,b,*], Nele Meyer [c], Andrey Rodionov [c], Claudia Knief [d], Michaela Aehnelt [e], Sara L. Bauke [a], Danh Biesgen [d], Stefan Dultz [f], Georg Guggenberger [f], Maguy Jaber [g], Erwin Klumpp [b], Ingrid Kögel-Knabner [h,i], Volker Nischwitz [j], Steffen A. Schweizer [h], Bei Wu [b], Kai U. Totsche [e], Eva Lehndorff [c]

[a] Institute of Crop Science and Resource Conservation – Soil Science and Soil Ecology, University of Bonn, Nussallee 13, 53115 Bonn, Germany
[b] Forschungszentrum Juelich GmbH, Agrosphere Institute – IBG3, Wilhelm Johnen Str., 52425 Juelich, Germany
[c] Soil Ecology, Bayreuth University, Dr.-Hans-Frisch-Str. 1-3, 95448 Bayreuth, Germany
[d] Institute of Crop Science and Resource Conservation – Molecular Biology of the Rhizosphere, University of Bonn, Nussallee 13, 53115 Bonn, Germany
[e] Institute of Geosciences – Hydrogeology, Friedrich Schiller University Jena, Burgweg 11, 07749 Jena, Germany
[f] Institute of Soil Science, Leibniz Universität Hannover, Herrenhäuser Str. 2, 30419 Hannover, Germany
[g] Sorbonne Université, LAMS (Laboratoire d'Archéologie Moléculaire et Structurale), UMR 8220, Institut Universitaire de France (IUF), 4 place Jussieu, F-75005 Paris, France
[h] Soil Science, TUM School of Life Sciences, Technical University of Munich, Emil-Ramann-Str. 2, 85354 Freising, Germany
[i] Institute for Advanced Study, Technical University of Munich, Lichtenbergstraße 2a, 85748 Garching, Germany
[j] Central Institute for Engineering, Electronics and Analytics, Analytics (ZEA-3), Forschungszentrum Juelich, Wilhelm Johnen Str., 52425 Juelich, Germany

ARTICLE INFO

Handling Editor: Cornelia Rumpel

Keywords:
Aggregate formation
Stable isotopes
Organo-mineral interactions
Extracellular polymeric substances
Iron oxides
Clay minerals

ABSTRACT

Microaggregates (<250 μm) are key structural subunits of soils. However, their formation processes, rates, and transformation with time are poorly understood. We took advantage of multiple isotope labelling of potential organic gluing agents and inorganic building units to unravel their role in soil aggregation processes being initiated with and without plant growth. We added ^{13}C-labelled extracellular polymeric substances (EPS), ^{15}N-labelled bacteria, ^{57}Fe-labelled goethite, and ^{29}Si-labelled montmorillonite to fine soil <250 μm of an Ap horizon from a Stagnic Luvisol, which was planted with *Festuca heteromalla* or kept bare in a climate chamber. Samples were taken after 4, 12, and 30 weeks, and separated into free (f) and occluded (o) microaggregates of different sizes (<20 μm, 53–20 μm, 250–53 μm), and in stable macroaggregates (>250 μm) that resisted 60 J mL^{-1} ultrasonic dispersion. Afterwards, we assessed the C, N, Fe, and Si stable isotope composition in each size fraction. After four weeks we found a rapid build-up of stable macroaggregates comprising almost 50 % of soil mass in the treatment with plants and respective soil rooting, but only 5 % when plants were absent. The formation of these stable macroaggregates proceeded with time. Soil organic carbon (SOC) contents were elevated by 15 % in the large macroaggregates induced by plant growth. However, the recovery of EPS-derived ^{13}C was below 20 % after 4 weeks, indicating rapid turnover in treatments both with and without plants. The remaining EPS-derived C was mainly found in macroaggregates when plants were present and in the occluded small microaggregates (<20 μm) when plants were absent. The excess of bacterial ^{15}N closely followed the pattern of EPS-derived ^{13}C ($R^2 = 0.72$). In contrast to the organic gluing agents, the goethite-^{57}Fe and montmorillonite-^{29}Si were relatively equally distributed across all size fractions. Overall, microaggregates were formed within weeks. Roots enforced this process by stabilizing microaggregates within stable macroaggregates. As time proceeded the labelled organic components decomposed, while the labelled secondary oxides and clay minerals increasingly contributed to aggregate stabilization and turnover at the scale of months and beyond. Consequently, the well-known hierarchical organization of aggregation follows a clear chronological sequence of stabilization and turnover processes.

* Corresponding author at: Institute of Crop Science and Resource Conservation – Soil Science and Soil Ecology, University of Bonn, Nussallee 13, 53115 Bonn, Germany.
E-mail address: wulf.amelung@uni-bonn.de (W. Amelung).

https://doi.org/10.1016/j.geoderma.2022.116226
Received 22 August 2022; Accepted 12 October 2022
Available online 22 October 2022

1. Introduction

Soils comprise a vast range of reactive surfaces. Many of them are involved in the formation of secondary particles of different size, initially micro-structured clay- and silt-sized organo-mineral associations (<20 μm; Six et al., 2004; Kögel-Knabner et al., 2008), and eventually microaggregates in the size range of 20–250 μm. Microaggregates exist in free form, others are occluded or even formed within larger particles like macroaggregates or peds (>250 μm; Six et al., 2000; Gulde et al., 2008; Totsche et al., 2018). The formation of aggregates and their potential hierarchical organization of increasing stability of structural entities with smaller sizes is well studied. The aggregate hierarchy is mediated by plants and fungal hyphae as well as by different organic gluing agents and inorganic building units (Totsche et al., 2018), which can be more or less developed depending on soil type and management (e.g., Tisdall and Oades, 1982; Six et al., 2004; Bronick and Lal, 2005; Kögel-Knabner and Amelung, 2021). However, little is still known on the formation pathways of microaggregates and on how the different processes of aggregate stabilization and turnover occur along temporal time scales.

Methodological progress in the past decades has provided information on element species associations, co-precipitates, and pore-size distributions in aggregates via nano-scale secondary ion mass spectrometry and synchrotron-based X-ray spectroscopy and microtomography, respectively (e.g., Lehmann et al., 2008; Vogel et al., 2014; Voltolini et al., 2017; Tamrat et al., 2019). Scanning electron microscopy, electron probe microanalyses, and laser ablation techniques extended these to the larger μm-scale (Chenu and Stotzky, 2002; Rodionov et al., 2019; Lehndorff et al., 2021). These methods substantiated earlier evidence that selected microaggregates may have a microbial nucleus (Foster, 1988; Ladd et al., 1993) or a mineral one (Dultz et al., 2019; Guhra et al., 2019), or that the adsorption of organic matter to minerals preconditions subsequent binding of minerals for microaggregate formation (Lehmann et al., 2007; Bucka et al., 2019, Guhra et al. 2019). Charge differences of the microaggregate forming materials are likely controlling these inorganic interactions, with clay minerals and Fe and Al oxyhydroxides being the main components involved (Pronk et al., 2012; Dultz et al., 2019; Guhra et al., 2019; Watts et al., 2005; Zech et al., 2020, Krause et al., 2020). In soil profiles the quantity of Fe and Al oxyhydroxides together with exchangeable Ca and pH served as better predictors of long-term SOC storage than clay minerals (Rasmussen et al., 2018).

Both plant- and microbial debris are common in mineral-associated organic matter (Angst et al., 2021). The study of Lehndorff et al. (2021) points to close associations between microbe- and plant-derived structures within soil microaggregates. The authors suggest that microbes feed on available C sources, thus producing additional gluing agents known to stabilize microaggregates (Tisdall and Oades, 1982; Cheshire, 1985). In this regard, plants may not only contribute to the stabilization of macroaggregates via root or associated mycorrhizal fungal growth (Jastrow et al, 1996; Six et al., 2000; Rillig, 2004), but the rhizosphere of plants is also region of increased bacterial growth and activity (Reinhold-Hurek et al., 2015; Kuzyakov and Blagodatskaya, 2015), and thus also for aggregation and microaggregate formation based on microbial gluing agents (Watteau et al., 2006; Wang et al., 2020; Guhra et al., 2022).

A large body of literature has accumulated on different aggregation mechanisms in soils, as summarized by, e.g., Oades (1988), Ladd et al. (1993), Six et al. (2004), Chenu and Cosentino (2011), Totsche et al. (2018), or Guhra et al. (2022). Nevertheless, we still lack a scheme to differentiate how different agents involved in particle bonding, such as extracellular polymeric substances (EPS; Tisdall and Oades, 1982; Kleber et al., 2007; Liu et al., 2013), bacterial residues (e.g., Ladd et al., 1993; Rodionov et al., 2001), oxyhydroxides (e.g., Oades and Waters, 1991; Krause et al., 2020), clay minerals (e.g., Chenu and Plante, 2006; Chenu and Cosentino, 2011; Schweizer et al., 2019), and other organic and inorganic soil constituents, which contribute to the initial formation, and subsequent turnover and transformation of different soil (micro-)aggregates (see Totsche et al., 2018, for a review). To understand how these different microaggregate forming materials interact in space and time, we have to monitor their fate in different aggregate size fractions over time.

Wang et al. (2020) stressed that roots accelerate aggregate turnover and occlusion of root-derived C. Also, several model experiments with the addition of organic gluing agents and inorganic building units have contributed to a better understanding of how aggregates are newly formed and in which size and density range they occur (e.g., Pronk et al., 2012; Krause et al., 2020; Wagai et al., 2020). Experiments on artificial soils indicated that different organic matter input materials, such as plant residues, dissolved organic matter, or bacterial necromass all induce the initial formation of aggregates within four weeks (Bucka et al., 2019, 2021), albeit to a different extent. Experiments with already existing aggregates used Dysprosium labelled prills (Plante et al., 1999), 1–3 mm ceramic spheres (Staricka et al., 1992) or rare earth oxides (DeGryze et al., 2006; Peng et al., 2017; Rahman et al., 2019) as tracers. Peng et al. (2017) added ^{13}C-glucose in addition to the rare earth oxides and found a linear relationship between turnover rate and amount of ^{13}C incorporated. The rare earth oxides incubated with microaggregates redistributed among different aggregate size fractions at an average rate of 30–88 days (DeGryze et al., 2006). Subsequent modelling extended the turnover time estimates of microaggregates to 181 days (Segoli et al., 2013). Hence, microaggregate turnover can be detected within a vegetation season, though these laboratory estimates indicate much faster aggregate turnover compared with chronosequence studies with prolonged arable management (e.g., Lobe et al., 2011) or arable land-use change to grassland (e.g. Jastrow, 1996; Li and Shao, 2006; Kösters et al., 2013), or compared with rates assessed for aggregate-associated organic matter as derived from natural ^{13}C abundance tracing (e.g., Puget et al., 2000) and radiocarbon analyses (Buyanovsky et al., 1994). Nevertheless, these labelling studies allowed to quantify the turnover of macroaggregates from the redistribution of the labels among different size fractions (DeGryze et al., 2006; Peng et al., 2017; Rahman et al., 2019), but hardly provided insight into aggregate forming mechanisms and how they interplay with other mechanisms of aggregate stabilization along temporal scales. Further, none of these studies so far revealed the rates at which different microaggregate forming materials affected the turnover of aggregates, because none of these studies additionally labelled the minerals of soils, such as hydroxides and phyllosilicates.

The concurrent action of different aggregate-forming mechanisms compromises the disentanglement of the action of the different gluing and cementing agents. Here, we aimed at overcoming this problem by assessment of the incorporation of ^{13}C-EPS, ^{15}N-bacteria, ^{57}Fe-FeOOH, and ^{29}Si-montmorillonite into micro- and macroaggregates formed from sieved soil (<250 μm) with and without plant growth. We hypothesized that (1) upon incubation with these organic gluing agents and inorganic bulding units, these microaggregate-forming materials are increasingly recovered in the occluded fraction. As plants promote the formation of stable macroaggregates and thus of occluded microaggregates by root exudation and microbial growth in the rhizosphere, we (2) assumed that the presence of plants diminishes the effect of the originally added EPS and bacteria. Due to their high reactivity, we further hypothesized that (3) montmorillonite, goethite, EPS, and bacteria bind rapidly to smaller microaggregates (<20 and <53–20 μm) because of their larger surface-to-volume ratio. Only over time, these may then aggregate to larger ones (53–250 μm). We finally hypothesized that (4) these biotic and abiotic aggregate forming agents do not only support the well-known spatial organization of (micro)aggregates, but also induce a temporal sequence in aggregate formation.

2. Materials and methods

To understand processes of initial soil aggregate formation and

turnover, a microcosm study was conducted in a climate chamber, using isotope-labelled organic and inorganic model compounds (^{13}C-EPS, ^{15}N-bacteria, ^{57}Fe-FeOOH, and ^{29}Si-montmorillonite) as major constituents of soil aggregate formation (Fig S1, Supplementary Materials).

For the production of ^{13}C-labelled EPS, we used *Bacillus subtilis* strain 168 [DSM 402], and employed a harvesting protocol as presented by Omoike and Chorover (2006). The bacterial cells were streaked onto fresh ^{12}C-glucose agar plates (glucose medium), cultured for 16 h under aerobic conditions, harvested, added to 50 mL ^{12}C glucose liquid medium, and were again allowed to grow overnight. Around 1–2 mL of the culture was transferred to 50 mL fresh ^{13}C-glucose medium and allowed to grow for 24 h. From this, again, 1–2 mL of the culture was added to new ^{13}C glucose medium (24 h of growth). This step was repeated up to four times to increase the incorporation of the ^{13}C-label. The cultures were harvested after 24 h of growth, i.e., in the stationary growth phase, when visibly maximum aggregation and viscosity occurred. EPS was separated from the cells by centrifugation (10,000×g, 4 °C). The pelleted cells were re-dispersed twice in the same supernatant; the final centrifugation step lasted 40 min. Finally, a volume reduction of the supernatant by 90 % was achieved using freeze-drying. The concentrated EPS was precipitated in cold ethanol (70 % of final concentration) for 12 h, and the precipitate was separated from the ethanol suspension by centrifugation (12,000×g, 30 min at 4 °C) and re-suspended in ultrapure (Milli-Q) water. This extraction was repeated 3 times (to obtain further precipitation of EPS in the supernatant). The pellet obtained after centrifugation was dissolved in Milli-Q water and dialyzed against Milli-Q water using Spectra/Por 7 regenerated cellulose (RC) membranes (1000 MWCO from Spectrum Europe, Breda, NL) to remove ethanol and entrained media residues. After dialysis for 72 h against two changes of Milli-Q water per day, the solution was freeze-dried to a dry, fibrous matrix and stored at −20 °C prior to use. Overall, ^{13}C-EPS was extracted with a mass yield of up to 400 mg L^{-1} of labelled EPS, which is in good agreement with Omoike and Chorover (2006) and Decho and Moriarty (1990), reporting yields of 420 mg L^{-1} and up to 3 g L^{-1}, respectively. Samples never exceeded 4 °C during the whole extraction procedure.

To obtain ^{15}N-labelled bacterial biomass, four different strains with specific characteristics regarding physiology, morphology and cell surface properties were selected as model organisms to reflect soil bacterial diversity: i) *Pseudomonas protegens* CHA0 gfp2 (Péchy-Tarr et al., 2013), a green fluorescence protein (GFP) labelled mutant of *Pseudomonas protegens* CHA0, which is a widely distributed, fast-growing soil bacterium with a broad substrate spectrum, ii) *Methylocystis parvus* DWT, a slow-growing soil bacterium not relying on soil organic carbon as a primary nutrient source, but on atmospheric methane, which enables cell maintainance for a couple of months (Knief & Dunfield, 2005), iii) *Streptomyces viridosporus* (DSM 40243^{T}) (Pridham et al., 1958), a soil bacterium characterized by its filamentous growth characteristics and its ability to degrade complex and hard-to-degrade carbon compounds such as lignin, and iv) *Gordonia alkanivorans* (DSM 44187) (Kummer et al., 1999), a soil bacterium characterized by its hydrophobic cell surface. P. *protegens* CHA0 gfp2 was cultivated in liquid culture on a shaker at 260 rpm in M9 medium (DSMZ medium 382) with the addition of gentamycin to ensure stable maintainance of the GFP label. *M. parvus* DWT was cultured on AMS medium (ATCC medium 784) agar plates under a 20 % (v/v) methane atmosphere. *S. viridosporus* was cultured on a shaker at 320 rpm in ISP4 liquid medium (DSMZ medium 547). *G. alkanivorans* was cultured on MSM solid medium (Rhee et al., 1998). All bacterial cultures were grown at 30 °C. The ^{15}N-labelling of bacterial cells was performed in AMS, MSM and M9 media by the addition of $^{15}NH_4Cl$ (≥98 atom % ^{15}N) (Sigma-Aldrich, St. Louis, USA) and in ISP4 medium by the addition of $(^{15}NH_4)_2SO_4$ (98 atom % ^{15}N) (Sigma-Aldrich, St. Louis, USA). On the starting day of the microcosm experiment, the bacterial cultures were harvested from plates or pelleted by centrifugation, re-suspended in sterile water and pooled. Due to its filamentous growth, the *S. viridosporus* culture was passed through a 150-μm mesh before being added to the final suspension. Each strain contributed with (25 % +/− 1.23) biomass (fresh weight) to the cell mixture. In the final mixture, 50.4 % of bacterial N was ^{15}N (Table 1).

For synthesis of ^{57}Fe labelled goethite, powdered ^{57}Fe metal with a degree of enrichment >95.5 % was obtained from EURISO-TOP (Saint Aubin, France). The Fe powder was dissolved in concentrated H_2SO_4 p. a., and Fe was oxidized to the trivalent form by addition of 30 % H_2O_2 for trace analysis (chemicals from VWR International GmbH, Darmstadt, Germany). Synthesis of goethite started by addition of 10 M NaOH under continuous stirring up to pH 12. The suspension was kept at 25 °C for 13 days (Cambier, 1986). After adjusting to pH 6 by addition of 0.1 M HCl, the goethite was washed with deionized water by centrifugation and decantation until the electrical conductivity was <20 μS cm^{-1}. Finally, the suspension was freeze-dried. The goethite crystallites showed needle-like habitus with an average needle length of 0.5 μm and an average thickness of 0.03 μm as determined by scanning electron microscopy (SEM; FEI Quanta 200, Hillsboro, USA) (Fig. S2a; Supplementary Materials). The purity of the goethite produced was verified by X-ray diffraction (XRD; CuKα radiation; 40 kV, 30 mA) using a Siemens D500 (Karlsruhe, Germany) instrument (Fig. S2b, Supplementary Materials). The specific surface area (SSA) measured by N_2 adsorption at 77 K (Quantachrome Nova 4000e, Boynton Beach, USA) was 75 ± 5 m^2 g^{-1}.

The ^{29}Si-labelled montmorillonite, $Ca_{0.2}(Al_{1.6}Mg_{0.4})[Si_4O_{10}(OH,F)_2]$, was synthesized according to the standard procedure for clay minerals outlined by Jaber et al. (2012) and Jacquemot et al. (2019), using 100 % of ^{29}Si labelled tetraethoxysilane (TEOS, CortecNEt, France) as silica source. The hydrogel was obtained by adding 25.1 mL of a solution of $Al(NO_3)_3$ (81.2 g L^{-1}) and 4.01 mL of a solution of $Mg(NO_3)_2$ (100.45 g L^{-1}) into a 15 mL solution of ethanol containing 0.1 mol of labelled TEOS and 0.005 mol of $CaCO_3$. An NH_4OH solution (33 %) was then added until gelification. The gel was stored one night at room temperature and heated one day at 200 °C and another day at 650 °C. The dried "gel" was then transferred into an internal silver tubing placed in an externally-heated Morey-type pressure vessel, where the montmorillonite was synthesized at a temperature of 400 °C, a water pressure of 1 kbar, and a duration of four weeks. The final product had a ^{29}Si label of about 10 % (Table 1), with a basal spacing of d001 = 1.4 nm, as typical for an expanding 2:1 type clay mineral (Fig. S3a, Supplementary Materials). The sharp d001 basal spacing evidences formation of desired size and crystallinity; transmission electron microscopy (TEM) confirms a voluminous structure prior to manual grinding (Fig. S3b, Supplementary Materials).

Microaggregates were obtained from the Ap horizon of a Stagnic

Table 1
Isotope abundances of N from bacteria, C from extracellular polymeric substances (EPS), Fe oxide and clay labels applied to the field-fresh soil fraction <250 μm of homogenized Ap horizon from a Stagnic Luvisol. Three gauze bags per pot were filled with labelled soil (3x13 g per pot; total labeled pots = 2x3x3). Added amounts of bactera are given in fresh biomass; respective calculations of added bacterial N are based on 13% N in dry bacterial biomass and 70% water content in fresh bacterial biomass.

	Added amount [g kg^{-1}]	Labeled representative	Isotope enrichment
Bacteria	27.75	^{15}N- *Pseudomonas protegens* ^{15}N- *Methylocystis parvus* ^{15}N-*Gordonia alkanivorans* ^{15}N- *Streptomyces viridosporus*	54.3 % ^{15}N of 1.082 g added N
EPS	1.22	^{13}C-EPS	3.7 % ^{13}C of 0.57 g added C
Oxide	0.456	$^{57}FeOOH*0.4H_2O$	95.5 % ^{57}Fe of 0.25 g added Fe
Clay	25.03	^{29}Si-montmorillonite	10 % ^{29}Si of 6.5 g added Si

Luvisol derived from loess (John et al., 2005), which was collected near Rotthalmünster, Germany, located in the Tertiary Hills (Tertiäres Hügelland) in the lower Rottal area. The soil had 17 % clay (<2 μm), 30 % fine silt (2–20 μm), 43 % coarse silt (20–63 μm) and 10 % sand (63–2000 μm); dominant minerals of the clay fraction were illite > kaolinite > vermiculite (John et al., 2005). Dry-sieving of the Ap soil sample to <250 μm was done to pre-destroy macroaggregates, as, e.g., also suggested by Guggenberger et al. (1999) and DeGryze et al. (2006) for aggregation experiments.

After synthesis, the EPS, goethite, and montomorillonite were freeze dried, sieved <250 μm and added in equal amounts to dry-sieved microaggregates (<250 μm). Thereafter, the ^{15}N bacterial suspension was added at a water content of 20 % w/w with a spray bottle, while constantly mixing the soil substrate. Table 1 provides details on the added amounts. The spiked soil was then filled into gauze bags with 13 g each and three bags were placed in the topmost 10 cm of a pot. The gauze (mesh size 1 mm) was selected to hinder coarse roots to enter the bags, but to allow ingrowth of fine roots and hyphae to support aggregate formation. Each treatment consisted of three pots. We thus prepared 18 pots, 9 of which were planted with *Festuca heteromalla* as a model plant (1 seed cm^{-2}). Additionally, 9 plant-free pots representing bare soil and additionally a total of 18 corresponding pots with unlabelled soils served as controls (see Fig. S1; Supplementary Materials for experiment details). All pots were incubated in a climate chamber under environmental conditions typical for summer in Germany (14 h daytime with 25 °C, 10 h night-time with 15 °C, 450 μmol m^{-2} s^{-1} light intensity, 70 % humidity). Artificial drip irrigation was applied in weekly intervals in order to prevent the pots from drying and to maintain soil moisture at 20 ± 3 % (w/w).

Soil samples were taken after 4 and 12 weeks of incubation and after one complete vegetation period of 30 weeks. *Festuca* has a dense root growth and is resistant against nutrient stress. Root growth was controlled by cutting the above-ground plant biomass (Volder et al., 2007) to about 10 cm after sampling at 4 and 12 weeks to prevent the formation of dense root balls in the pots that would complicate obtaining complete macro- and microaggregates even when protected from coarse roots in gauze bags.

2.1. Physical fractionation

Microaggregates can be analytically released from macroaggregates using a certain ultrasonic energy input for dispersion (usually 60 J mL^{-1}; Amelung and Zech, 1999; Kaiser and Berhe, 2014). Two of the gauze bags from each pot were combined for aggregate fractionation to obtain sufficient material for chemical analyses, the third gauze bag set was fractionated separately for microbial analyses. For both sets, soil aggregates were fractionated by wet sieving as described by Krause et al. (2018). In brief, 20 g mixed from 10 g each from two gauze bags was fresh-sieved to 8 mm, and then slaked in 150 mL water on a 250-μm sieve to obtain the weakly associated, so-called free microaggregates, which were further separated into size classes in the range of 250–53 μm, 53–20 μm, and <20 μm by passing through a sieve tower (denoted as f 250-53 μm, f 53-20 μm, f <20 μm, respectively). All remaining macroaggregates were then ultrasonically dispersed at 60 J mL^{-1} (Branson Ultrasonics corp., Connecticut, USA), which according to Stemmer et al. (1998, 1999) and Amelung and Zech (1999) should largely destroy the macroaggregates without impairing microbial life. From these we obtained the occluded microaggregates, again in the size ranges of 250–53 μm, 53–20 μm, <20 μm, and denoted as o 250-53 μm, o 53-20 μm, and o <20 μm fraction, respectively. Noteworthy, however, the dispersion of the macroaggregates was not complete. Hence, we additionally sampled the remaining stable macroaggregate fraction (stable against 60 J mL^{-1} energy input) in the size ranges of 8000–2800, 2800–2000, 2000–500, and 500–250 μm by passing through a sieve tower.

For microbial analyses, samples were stored at 4 °C and processed within a few days in the same way. Aggregates were collected in reaction tubes, excess water removed and samples stored at −20 °C until DNA extraction. For chemical analyses, all aggregate fractions were cryo-stabilized by shock frosting in liquid nitrogen and freeze-dried as recommended by Siebers et al. (2018). The microorganisms were inactivated in these samples by γ-irradiation (BBF Sterilisationsservice GmbH, Kernen, Germany). The mean recovery was 96.2 ± 3.1 % of the original soil mass. No sand corrections were performed due to limitations in sample weight. For the same reason, the stable macroaggregate fractions <2800 μm were pooled for isotope analyses.

2.2. Chemical element and isotope analyses

Total carbon and nitrogen were determined after dry combustion using a CNS analyser (Vario EL, Elementar, Hanau, Germany). The respective stable isotope composition was assessed on an isotope ratio mass spectrometer (visION, Elementar, Hanau, Germany) coupled to an elemental analyzer (pyro cube, Elementar, Hanau, Germany). ^{13}C abundances were expressed in δ notation in per mill relative to the Pee Dee Belemnite standard ($\delta^{13}C_{VPDB}$), and ^{15}N abundances were expressed as $\delta^{15}N$ in per mill relative to atmospheric N_2 ($\delta^{15}N_{atm}$). For assessing the ^{15}N enrichment in bacterial cell mixtures, the labelled material was measured at 100-fold dilution by mass with unlabelled cell biomass. The distribution of elements and ion species was analyzed using a NanoSIMS 50L (Cameca, Gennevilliers, France) of the individual components on indium-tin-oxide (ITO) wafers (Fig. S4a,b; Supplementary Materials). The results confirmed the successful addition of intended labels and revealed substantial heterogeneity of the ^{15}N and particularly of the ^{13}C and ^{29}Si labels within the added components, while the distribution of ^{57}Fe in the goethite was rather homogeneous (Fig. S4a,b; Supplementary Materials).

For extraction of total Fe and Si, 20 mg of each size fraction were mixed with 0.5 g NaOH in an Au-crucible and fusion was performed at 500 °C in a muffle furnace for 30 min. After cooling, the melt was dissolved by addition of deionized water in several steps. The resulting solutions were acidified with 5 % HCl and made up to 50 mL. Fe and Si concentrations were determined by inductively coupled plasma optical emission spectroscopy (ICP-OES, iCAP, Thermo Fisher Scientific, Bremen, Germany) and $^{57}Fe/^{56}Fe$ and $^{29}Si/^{28}Si$ ratios by sector-field inductively coupled plasma mass spectrometry (SF-ICP-MS, Element 2, Thermo Fisher Scientific, Bremen, Germany), respectively. To eliminate the spectral interferences the ratios were measured in the medium mass resolution mode (R = 4000). To reduce the Si background, the measurements of $^{29}Si/^{28}Si$ ratios were performed after several hours of purging and matrix adapted blank measurements until stable background intensities of Si (i.e. the analytical blank) were achieved. The analytical blank was monitored after every-five or seven individual measurements. To monitor and correct the signal drift, a strategy of "standard-sample-standard" bracketing was applied for the ratio measurements, where an Fe (Fe isotope standard IRMM-014) and a Si standard (naturally abundant Si ICP-MS standard) was measured before and after each sample, respectively. The true $^{57}Fe/^{56}Fe$ and $^{29}Si/^{28}Si$ ratios of each sample were then calculated via the δ values in per mil against the measured standards.

2.3. Assessment of bacterial abundance by quantitative PCR

DNA extraction was done using the NucleoSpin Soil Kit (Macherey Nagel, Düren, Germany) as described earlier (Biesgen et al., 2020). A specific qPCR assay was developed for each of the four strains. The qPCR assays were prepared and DNA amplified as described by Frindte et al. (2020). Specific details about primers and cycling conditions are given in Table S1, Supplementary Materials. To determine soil dry weight, lysis tubes were weighed before use and after DNA extraction and soil drying.

2.4. Calculations

By convention, the ^{13}C and ^{15}N abundance in a sample is expressed in delta-units ($\delta^{13}C‰$ or $\delta^{15}N‰$):

$$\delta^{13}C‰ \; or \; \delta^{15}N‰ \; = \; (R_{Sam}/R_{Std}) \; - \; 1) \; x \; 1000, \tag{1}$$

where R_{Sam} is the $^{13}C/^{12}C$ or $^{15}N/^{14}N$ isotope ratio of the sample. R_{Std} referred to the $^{13}C/^{12}C$ isotope ratio of the international Pee Dee Belemnite standard for C and to the ^{15}N natural abundance in the atmosphere for N.

For Si and Fe isotopes, individual measured raw ratios were first converted to the δ notation using the following equation:

$$\delta(‰) = \left(\frac{R_{raw}}{\left(\frac{R_{std-b}+R_{std-a}}{2}\right)} - 1 \right) \times 1000 \tag{2}$$

where R_{raw} was the measured raw molar ratio of $^{29}Si/^{28}Si$, $^{57}Fe/^{56}Fe$, respectively, of the sample, and $R_{std\text{-}b}$ and $R_{std\text{-}a}$ were the measured ratios of respective standard determined before and after the sample. R_{raw} was then corrected with the known isotope ratio of the standard R_{std} to obtain the correct ratio of the sample R_{sam} by using:

$$R_{sam} = \left(\frac{\delta}{1000} + 1\right) \times R_{std} \tag{3}$$

For C and N, the abundance (Ab) of the tracer isotope (Ab_t), i.e., ^{13}C and ^{15}N, respectively, was calculated by applying:

$$Ab_t(\%) = \frac{R_{sam}}{R_{sam}+1} \times 100 \tag{4}$$

The atomic percent excess (APE) of the tracer isotope in the sample was the difference between the enriched abundance Ab_t and the natural abundance $Ab_{nat\text{-}t}$, assessed from the unlabelled control plots.

$$APE_t(\%) = Ab_t - Ab_{nat-t} \tag{5}$$

For Fe and Si, in addition to the tracer isotope, i.e., ^{57}Fe and ^{29}Si, respectively, it has to be considered that two or more non-tracer stable isotopes were present at natural abundance. Therefore, the abundance of ^{57}Fe and ^{29}Si was calculated using:

$$Ab_{^{57}Fe}(\%) = \frac{R_{sam}}{R_{nat\left(^{54}Fe/^{56}Fe\right)} + 1 + R_{sam} + R_{nat\left(^{58}Fe/^{56}Fe\right)}} \times 100 \tag{6}$$

and

$$Ab_{^{29}Si}(\%) = \frac{R_{sam}}{1 + R_{sam} + R_{nat\left(^{30}Si/^{28}Si\right)}} \times 100 \tag{7}$$

respectively, where R_{nat} is the natural isotope ratio of $^{54}Fe/^{56}Fe$, $^{58}Fe/^{56}Fe$, and $^{30}Si/^{28}Si$, respectively. The abundance of each isotope of Fe and Si was calculated in the same manner. For instance,

$$Ab_{^{56}Fe}(\%) = \frac{1}{R_{nat\left(^{54}Fe/^{56}Fe\right)} + 1 + R_{sam} + R_{nat\left(^{58}Fe/^{56}Fe\right)}} \times 100 \tag{8}$$

$$Ab_{^{28}Si}(\%) = \frac{1}{1 + R_{sam} + R_{nat\left(^{30}Si/^{28}Si\right)}} \times 100 \tag{9}$$

Subsequently, the molar mass of the enriched element M_E was obtained by:

$$M_E\left(g\ mol^{-1}\right) = \sum \left(m_i \times Ab_i\right) \tag{10}$$

where m_i and Ab_i are the atomic mass and the abundance of the isotope i in the element E, respectively.

Assuming the content of total element (C_E, in g kg^{-1}) in the control samples was the same as that in the samples, the excess content of the tracer isotope ΔC_t in the sample was calculated by comparing its content in the sample with that in the control samples by using:

$$\Delta C_t \left(g\ kg^{-1}\right) = \left(\frac{C_E}{M_E} \times Ab_t - \frac{C_E}{M_{ref}} \times Ab_{ref-t}\right) \times m_t \tag{11}$$

where m_t is the atomic mass of the tracer isotope t (i.e., ^{13}C, ^{15}N, ^{29}Si and ^{57}Fe) and M_{ref} is the molar mass of the element with the tracer isotope t at an abundance of $Ab_{ref\text{-}t}$. In our case, this reference abundance of the tracer isotope was as follows for the individual elements, respectively: the mean value of ^{13}C abundance in the control samples ($Ab_{ck\text{-}13C}$ = 1.08507573 %), the atmospheric ^{15}N abundance ($Ab_{atm\text{-}15N}$ = 0.36897303 %), the certified amount fraction of ^{57}Fe in IRMM-014 ($Ab_{IRMM\text{-}014\text{-}57Fe}$ = 2.1192 %) and the natural abundance of ^{29}Si ($Ab_{nat\text{-}29Si}$ = 4.685 %). It should be noted that in this approach errors may derive both from error propagation when summing up tracer levels across all aggregate fractions for recovery estimates, as well as from deviations in natural isotope abundances in individual aggregate fractions from the average backgrounds of the bulk soil, and this effect may be more pronounced for tracers with small labelling levels. Noteworthy both natural ^{57}Fe and ^{29}Si natural abundances may change with different degree of weathering (Wu et al., 2019a; Opfergelt and Delmelle, 2012), which is unknown for the different aggregate fractions.

2.5. Assessment of aggregate turnover

We analysed the four different isotope labels in seven size fractions at three sampling times, i.e., over two time intervals. We thus have more data points for each isotope label in different size fractions than in different time intervals, which precluded a quantitative assessment of gross microaggregate formation and turnover rates. Also, some macroaggregates were not fully dispersed when obtaining occluded microaggregate fractions. Here we thus focus on the relative distribution of the isotope labels across the different size classes over time to compare the effect of the different aggregate-forming materials on (micro) aggregate abundance and stability, and we used shifts in aggregate weight and isotope labels as indicators of net turnover rates.

2.6. Statistical analyses

We used linear mixed-effect models with size fraction, sampling time, and treatment as fixed effects and pot ID as random effect. We also tested for interactions. This was performed in R (version 3.6.1, R Core Team, 2020) using the function *lme* available in the nlme package (Pinheiro et al., 2017). In case of significant effects, post-hoc tests were applied to investigate (i) differences between size fractions for each treatment and sampling time, (ii) differences between sampling times for each size fraction and treatment, and (iii) differences between treatments for each size fraction and sampling time. This was done using the function *lsmeans* of the lsmeans package (Lenth, 2018) with Tukey adjustment for multiple comparisons. Data were checked for normal distribution of residuals by visual inspection of histograms and QQplots. Variance homogeneity was tested with Levene's test. As linear mixed effect models have been demonstrated to be robust against moderate violations of distributional assumptions (Schielzeth et al., 2020), we decided to keep the model even in case of slight deviations. The qPCR data were analyzed by ANOVA with the factor strain included as additional factor, but without pot ID because of some missing data (cell numbers below detection limit). Further, the sum of strains was analyzed using a linear mixed effect model as described above, but with the following modifications: the effect of treatment was first tested excluding the 8000–2800 μm fraction as those data were largely missing in the bare treatment. Differences between fractions where then tested for the planted treatment and the bare treatment separately. This was done to include macroaggregates in the model of the planted treatment.

Differences were considered as significant for $p < 0.05$. Correlations were tested using Excel for Windows, Office version 16.

3. Results

3.1. Aggregate dynamics

The field-fresh soil used for the multi-isotope labelling incubation experiment comprised mainly microaggregates occluded in macroaggregates (>50 % of soil mass); however, 13.5 % of the soil aggregates resisted ultrasonic dispersion of 60 J mL^{-1} and thus ended up in the stable macroaggregate fraction (Table 2, bottom). For the incubation experiment, the soil material had been sieved <250 μm; i.e., there were only microaggregates and primary particles present at the start of the incubation period. At the first sampling point and in the bare soil, the size distribution of these microaggregates resembled that of the field-fresh soil, except for the f 250-53 μm fraction, for which the relative mass contribution tripled compared with the field-fresh soil, while stable macroaggregates hardly existed (Table 2).

This size distribution changed significantly over time, and it was largely affected by the presence of plants, showing intensive root development towards the end of the experiment (Fig. S6; Supplementary Materials). It should be recalled that the aggregate fractionation here is operationally defined, i.e., each aggregate fraction may contain also primary particles. This was particularly evident for the "free" particle and microaggregate fraction of the bare soil treatment (Fig. S7; Supplementary Materials). "Free" in this context means that the particles and microaggregates were not included in macroaggregates. It does not preclude an inclusion of small microaggregates into larger microaggregates.

By definition, as added, all microaggregates were "free" when the experiment started. In the treatments without plants, about 70 % of these free aggregates did not remain in this free form, but accumulated in the occluded fraction after four weeks, particularly in the two occluded (o) fractions o <20 μm and o 53-20 μm (51.4 % of soil mass; Table 2). The amount of newly formed occluded aggregates within four weeks allows a first estimation on formation rates. A formation of 82 g occluded microaggregates o 250–53 μm in the bare soil treatments in 4 weeks thus corresponds to a linearized formation rate of 20 g kg^{-1} soil per week for the o 250-53 μm fraction, while formation of the finer o <20 μm and o 53–20 μm fractions was 3–4 times faster, respectively. Macroaggregates were also formed, though at slower rates: 11 g kg^{-1} soil $week^{-1}$ for macroaggregates in the size range of 2000 to 250 μm, slowing down to 1–2 g kg^{-1} soil $week^{-1}$ for macroaggregates >2800 μm and 2800–2000 μm, respectively (Table 2).

As time proceeded, the pool of free microaggregates continued to decline, so that after 30 weeks 80 % of soil mass accumulated in other aggregate fractions. Yet, this accumulation did at this time point not only occur within occluded microaggregates but also within stable macroaggregates. The occluded microaggregate fraction o 250-53 μm gained 45 % of its weight, finally comprising 119 g kg^{-1} soil after 30 weeks. The other two occluded microaggregate fractions lost 32–43 % of their weight compared with the 4-week scenario. In contrast, weight was gained by stable macroaggregates of all sizes. When averaged across the experiment duration, in the bare soil treatments net formation rates of stable macroaggregates were from 66 g in 30 weeks, i.e., 2.2 g macroaggregates kg^{-1} soil $week^{-1}$, for the 8000–2800 μm fraction, 43 g in 30 weeks = 1.4 g macroaggregates kg^{-1} soil $week^{-1}$ for the 2800–2000 μm fraction, and 4.7 and 2.4 g macroaggregates kg^{-1} soil $week^{-1}$, for the two smaller stable macroaggregate fractions 2000–500 μm and 500–250 μm (Table 2).

In the treatments with *Festuca* plants, more occluded particles and microaggregates (ca. 30 % of soil weight) and stable macroaggregates (almost 50 % of soil weight) were formed than in the bare soil treatments within the four weeks since experiment start, even exceeding the amount observed in the field-fresh soil (Table 2). The presence of plants

Table 2
Size distribution of free (f) and occluded (o) particles and microaggregates in field-fresh soil as well as after 4, 12, and 30 weeks of incubating <250 μm sieved soil with additions of isotopically labelled extracellular polymeric substances (EPS), selected bacterial strains, goethite and montmorillonite with and without presence of *Festuca* plants. Data are given as mean (n = 3) ± standard deviation. Different lowercase letters indicate significant differences between fractions within a given treatment and sampling time. Different capital letters indicate significant differences between sampling times within a given treatment and size fraction. An asterisk indicates a significant difference between treatments (*Festuca* plants vs bare soil) within a given size fraction and sampling time. Comparisons where no letters or asterisks are indicated did not show significant differences.

Fraction	Treatment	Size distribution (%)		
		after 4 weeks	after 12 weeks	after 30 weeks
Macroaggregates				
8000–2800 μm	bare soil	$0.4 \pm 0.4^{a*}$	$4.4 \pm 6.6^{ab*}$	$6.6 \pm 3.6^{ab*}$
2800–2000 μm	bare soil	0.7 ± 0.6^{a}	2.5 ± 1.7^{a}	4.3 ± 1.2^{a}
2000–500 μm	bare soil	2.6 ± 1.6^{abA}	10.3 ± 4.7^{abcB}	14.2 ± 2.1^{bcB}
500–250 μm	bare soil	1.8 ± 1.3^{ab}	6.4 ± 1.7^{ab}	7.2 ± 0.8^{ab}
Microaggregates + primary particles				
o 250–53 μm	bare soil	8.2 ± 2.1^{abc}	$11.9 \pm 1.2^{bc*}$	$11.9 \pm 0.5^{ab*}$
o 53–20 μm	bare soil	$29.6 \pm 3.7^{eB*}$	$25.1 \pm 5.4^{dAB*}$	$20.1 \pm 2.8^{cA*}$
o <20 μm	bare soil	$21.8 \pm 0.9^{deB*}$	$16.4 \pm 4.5^{cAB*}$	$12.6 \pm 3.0^{bcA*}$
f 250–53 μm	bare soil	$15.0 \pm 5.6^{cd*B}$	7.7 ± 2.2^{abA}	8.1 ± 0.5^{abA}
f 53–20 μm	bare soil	9.3 ± 2.5^{bc}	6.9 ± 2.3^{ab}	8.1 ± 0.7^{ab}
f <20 μm	bare soil	4.8 ± 1.9^{ab}	3.1 ± 0.7^{a}	4.3 ± 0.7^{a}
Material recovery		94.5 ± 4.1	94.6 ± 0.6	97.3 ± 1.0
Macroaggregates				
8000–2800 μm	with plants	$42.4 \pm 7.6^{eA*}$	$52.7 \pm 3.3^{bB*}$	$37.6 \pm 12.1^{dA*}$
2800–2000 μm	with plants	0.2 ± 0.1^{a}	1.3 ± 0.0^{a}	1.5 ± 0.1^{a}
2000–500 μm	with plants	2.8 ± 0.9^{abA}	7.5 ± 0.4^{aAB}	12.9 ± 4.3^{cB}
500–250 μm	with plants	3.9 ± 0.9^{abc}	2.8 ± 0.4^{a}	5.4 ± 2.1^{abc}
Microaggregates + primary particles				
o 250–53 μm	with plants	10.9 ± 2.3^{cdB}	$4.2 \pm 0.6^{aA*}$	$5.1 \pm 1.5^{abcAB*}$
o 53–20 μm	with plants	$13.7 \pm 2.7^{d*}$	$8.5 \pm 1.2^{a*}$	$8.9 \pm 1.8^{abc*}$
o <20 μm	with plants	$6.5 \pm 1.2^{abcd*}$	$4.7 \pm 0.9^{a*}$	$5.4 \pm 0.5^{abc*}$
f 250–53 μm	with plants	$8.5 \pm 2.1^{bcd*}$	3.8 ± 0.9^{a}	6.0 ± 1.8^{abc}
f 53–20 μm	with plants	9.4 ± 4.6^{bcd}	6.9 ± 1.5^{a}	10.9 ± 2.9^{bc}
f <20 μm	with plants	4.2 ± 2.2^{abc}	4.2 ± 1.0^{a}	4.6 ± 0.3^{ab}
Material recovery		102.5 ± 3.8	96.7 ± 2.6	98.2 ± 1.6
Initial aggregate size distribution at the time of sampling				
Macroaggregates				
8000–2800 μm	Field soil	9.8 ± 4.4		
2800–2000 μm	Field soil	1.0 ± 0.3		
2000–500 μm	Field soil	1.8 ± 0.2		
500–250 μm	Field soil	0.9 ± 0.0		
Microaggregates + primary particles				
o 250–53 μm	Field soil	8.3 ± 1.7		
o 53–20 μm	Field soil	31.2 ± 2.5		
o <20 μm	Field soil	19.6 ± 2.0*		
f 250–53 μm	Field soil	4.1 ± 1.3*		
f 53–20 μm	Field soil	8.1 ± 3.2		
f <20 μm	Field soil	4.6 ± 1.4		
Material recovery		89 ± 0.7		

and related rooting thus accelerated the formation of macroaggregates, particularly of the stable, large ones (8000–2800 μm): the formation rates of the latter increased by a factor of 100 from 1 g kg^{-1} soil $week^{-1}$ in the bare soil to 106 g kg^{-1} soil $week^{-1}$ in the planted soil when only considering the first 4 weeks of experiment (Table 2). Yet, the amount of occluded particles and microaggregates was smaller in the planted soil than in the bare soil (Table 2), reflecting that a significant portion of stable soil macroaggregates had endured standard ultrasonic disintegration at 60 J mL^{-1} when roots were present.

As time proceeded, the pool of occluded particles and microaggregates declined in both treatments (Table 2). In the planted soil, this decline already ceased after 12 weeks. In contrast, there was a temporary maximum of the 2800–2000 μm stable macroaggregate fraction, and a continuous build-up of the smaller macroaggregate fractions (significant for the 2000–500 μm fraction; Table 2). Hence, stable macroaggregate formation slowed down but did not cease during the experimental period of 30 weeks.

3.2. Element contents

The <250 μm fraction used to set up the incubation experiment had an SOC content of 11.6 ± 0.3 g kg^{-1}, similar to the SOC content found in the planted soil (Table 3). The SOC contents varied clearly among fractions and between treatments (interaction terms significant; Table 3) but changed little over time (significant only for the o 53-20 μm and macroaggregate fraction, Table 3). In the bare soil treatments, the largest SOC contents were found in occluded microaggregates o <20 μm, while the SOC contents in the other occluded fractions were similar to those of free microaggregates f <20 μm and f 53-20 μm; the SOC contents in stable macroaggregates increased over time ($p < 0.05$; Table 3). This pattern was similar but less pronounced when plants were present. Nevertheless, plant growth raised C contents relative to the bare soil in the o <20 μm and stable macroaggregate fraction 8000–2800 μm (they contained elevated SOC contents expressed in g C kg^{-1} soil; Table 3). The smallest SOC contents in the presence of plants occurred again in the 53–20 μm particle and microaggregate fractions, both for the free and occluded materials. The largest SOC contents occurred in the free particles and microaggregates f <20 μm (similar to the range in SOC contents of the bare soil treatment), as well as in the stable macroaggregates, as already indicated (Table 3). Overall, SOC contents varied by up to a factor of 8 among fractions, whereas temporal changes within a given fraction hardly exceeded a factor of 1.5.

The variation in the contents of total Fe and Si among fractions was much smaller, however, still reaching at maximum a factor of 3.1 for Fe and a factor of 1.8 for Si. The largest Fe contents occurred in the <20 μm fractions, and the smallest ones in the 53–20 μm fractions, both of the free and occluded particles and microaggregates (Table S2, Supplementary Materials). The Fe contents in stable macroaggregates were intermediate. This pattern was similar for the treatments with and without plants; yet, after 30 weeks, o 250-53 μm and o 53-20 μm fractions of the treatment with plants had smaller Fe contents than the bare soil ones (Table S2; Supplementary Materials).

Over time, contents of total Fe remained fairly constant for most of the fractions: in both treatments with and without plants, the Fe contents in the free particle and microaggregate fractions declined with time (significant for the f 250-53 μm fraction in the bare soil treatment as well as for f 53-20 μm and f <20 μm fractions in the planted treatment; Table S2, Supplementary Materials). Even if there was no concomitant increase in Fe content in the other fractions, these losses went along with increases in the total mass of stable macroaggregates (Table 2) and thus with the total amount of Fe in this fraction, indicating a relocation of Fe-containing soil mass into stable macroaggregates.

The distribution of total Si among the size fractions tended to oppose that of Fe, but generally reflected the texture of minerals, with clays being rich in Si and attached Fe and sand particles being rich in Si only. Smaller Si contents tended to occur in the o <20 μm fractions, and larger

Table 3
Soil organic carbon (SOC) distribution among free (f) and occluded (o) particles and microaggregates as well as of macroaggregates after 4, 12, and 30 weeks of incubating <250 μm sieved soil with additions of isotopically labelled extracellular polymeric substances (EPS), bacteria, goethite and montmorillonite, and with and without presence of *Festuca* plants. Different lowercase letters indicate significant differences between fractions within a given treatment and sampling time. Different capital letters indicate significant differences between sampling times within a given treatment and size fraction. An asterisk indicates a significant difference between treatments (*Festuca* plants vs bare soil) within a given size fraction and sampling date. Comparisons where no letters or asterisks are indicated did not show a significant difference.

Fraction μm	Treatment	SOC concentration (g kg^{-1} fraction)			SOC content (g kg^{-1} soil)		
		after 4 weeks	after 12 weeks	after 30 weeks	after 4 weeks	after 12 weeks	after 30 weeks
Macroaggregates							
8000–2800	bare soil	11.0 ± 6.4 ^{bA*}	12.0 ± 1.0 ^{bB}	11.1 ± 0.1 ^{bB*}	0.04 ± 0.04 ^{a*}	0.50 ± 0.75 ^{a*}	0.73 ± 0.40 ^{ab*}
2800–250	bare soil	11.8 ± 0.5 ^{cd}	12.0 ± 0.1 ^{b}	11.5 ± 0.1 ^{b}	0.59 ± 0.42 ^{abA}	2.29 ± 0.95 ^{bcB}	2.93 ± 0.40 ^{cB}
Microaggregates + primary particles							
o 250–53	bare soil	8.2 ± 1.2 ^{bcA}	12.2 ± 3.0 ^{bB}	10.8 ± 0.5 ^{bAB}	0.69 ± 0.25 ^{ab}	1.45 ± 0.32 ^{ab*}	1.28 ± 0.07 ^{ab}
o 53–20	bare soil	2.1 ± 0.2 ^{a*}	3.8 ± 0.7 ^{a}	3.8 ± 0.4 ^{a}	0.63 ± 0.10 ^{ab}	0.94 ± 0.09 ^{a}	0.76 ± 0.04 ^{ab}
o <20	bare soil	16.8 ± 1.5 ^{e*}	17.0 ± 2.1 ^{c*}	14.6 ± 0.6 ^{b}	3.67 ± 0.37 ^{cB*}	2.84 ± 1.07 ^{cAB*}	1.85 ± 0.51 ^{bcA*}
f 250–53	bare soil	12.6 ± 1.1 ^{d}	12.7 ± 0.3 ^{b}	11.4 ± 0.2 ^{b}	1.85 ± 0.54 ^{b}	0.98 ± 0.28 ^{a}	0.92 ± 0.04 ^{ab}
f 53–20	bare soil	7.2 ± 0.4 ^{b}	6.9 ± 0.2 ^{a}	6.4 ± 0.3 ^{a}	0.66 ± 0.15 ^{ab}	0.48 ± 0.17 ^{a}	0.52 ± 0.05 ^{a}
f <20	bare soil	14.4 ± 1.5 ^{de}	13.2 ± 0.2 ^{b}	12.9 ± 1.3 ^{b}	0.53 ± 0.12 ^{ab}	0.41 ± 0.09 ^{a}	0.55 ± 0.08 ^{a}
Sum					*8.7 ± 1.2*	*9.9 ± 0.9*	*9.5 ± 0.8*
Macroaggregates							
8000–2800	with plants	12.7 ± 0.3 ^{c*}	14.0 ± 0.3 ^{bc}	14.6 ± 1.1 ^{b*}	5.37 ± 0.97 ^{b*A}	7.39 ± 0.62 ^{b*B}	5.54 ± 2.04 ^{b*A}
2800–250	with plants	13.1 ± 0.6 ^{c}	14.0 ± 0.1 ^{bc}	13.6 ± 0.3 ^{b}	0.89 ± 0.22 ^{aA}	1.63 ± 0.10 ^{aAB}	2.69 ± 0.88 ^{cB}
Microaggregates + primary particles							
o 250–53	with plants	10.6 ± 3.4 ^{abc}	11.5 ± 2.3 ^{bc}	11.5 ± 1.1 ^{b}	1.10 ± 0.23 ^{a}	0.49 ± 0.16 ^{a*}	0.59 ± 0.24 ^{a}
o 53–20	with plants	8.4 ± 4.5 ^{abB*}	4.9 ± 0.6 ^{aA}	4.4 ± 0.3 ^{aA}	1.21 ± 0.87 ^{a}	0.41 ± 0.08 ^{a}	0.39 ± 0.05 ^{a}
o <20	with plants	11.7 ± 0.5 ^{bc*}	12.7 ± 0.3 ^{bc*}	11.9 ± 1.4 ^{b}	0.76 ± 0.17 ^{a*}	0.60 ± 0.12 ^{a*}	0.64 ± 0.13 ^{a*}
f 250–53	with plants	11.9 ± 0.1 ^{bc}	10.8 ± 1.3 ^{b}	12.8 ± 0.6 ^{b}	1.02 ± 0.24 ^{a}	0.41 ± 0.14 ^{a}	0.77 ± 0.26 ^{a}
f 53–20	with plants	7.0 ± 1.5 ^{a}	6.0 ± 0.9 ^{a}	6.0 ± 0.1 ^{a}	0.67 ± 0.38 ^{a}	0.42 ± 0.15 ^{a}	0.65 ± 0.18 ^{a}
f <20	with plants	13.3 ± 0.6 ^{c}	14.7 ± 0.7 ^{c}	13.9 ± 0.7 ^{b}	0.56 ± 0.30 ^{a}	0.62 ± 0.13 ^{a}	0.64 ± 0.04 ^{a}
Sum					*11.6 ±1.6*	*12.0 ± 2.4*	*11.9 ± 1.8*

ones in the larger fractions, as a trend for both the free and occluded particles and microaggregates, but significant only after 30 weeks for the difference between microaggregates and stable macroaggregates in the bare soil treatment as well as larger occluded microaggagates or stable macroaggregates and free microaggregates, respectively (Table S2; Supplementary Materials). Plants affected the Si distribution between fractions only in later stages of the experiment, where larger Si contents (similar to larger Fecontents) were found after 30 weeks for the o 250-53 μm and o 53-20 μm fraction in the treatment with plants than in those without (Table S2; Supplementary Materials). Also, Si contents declined with time in the f 53-20 μm fraction of the planted soil and in occluded fractions in bare soil (Table S2; Supplementary Materials).

3.3. Fate of ^{13}C-labelled EPS

The EPS-derived ^{13}C accumulated primarily in the <20 μm fractions, and showed lowest concentrations in the o 53-20 μm fraction ($p < 0.05$; Fig. 1, left). Fractions with largest contents of SOC (Table 3) thus also showed maximum ^{13}C excess, documenting that these fractions have properties that facilitated SOC and EPS accrual. Substantial amounts of ^{13}C, however, were also found in the stable macroaggregate fractions (Fig. 1, left), the diameter of which exceeds by far the average molecular chain length of EPS. After 12 weeks, excess ^{13}C peaked in the occluded microaggregates o <20 μm of the bare soil treatment, which went along with increasing ^{13}C accrual in these fractions. This enrichment was missing in the planted treatments (indicated by the asterisks in Fig. 1, right). Besides, the degree of this ^{13}C accrual in the o <20 mm fractions of the bare soil declined after 30 weeks (Fig. 1, right). Similarly, as time proceeded, excess ^{13}C declined in nearly all size fractions (capital letters; Fig. 1, left).

It is worth noting that the recovery of EPS-derived ^{13}C was below 10 % of the added amount, i.e., the majority of this label had been lost

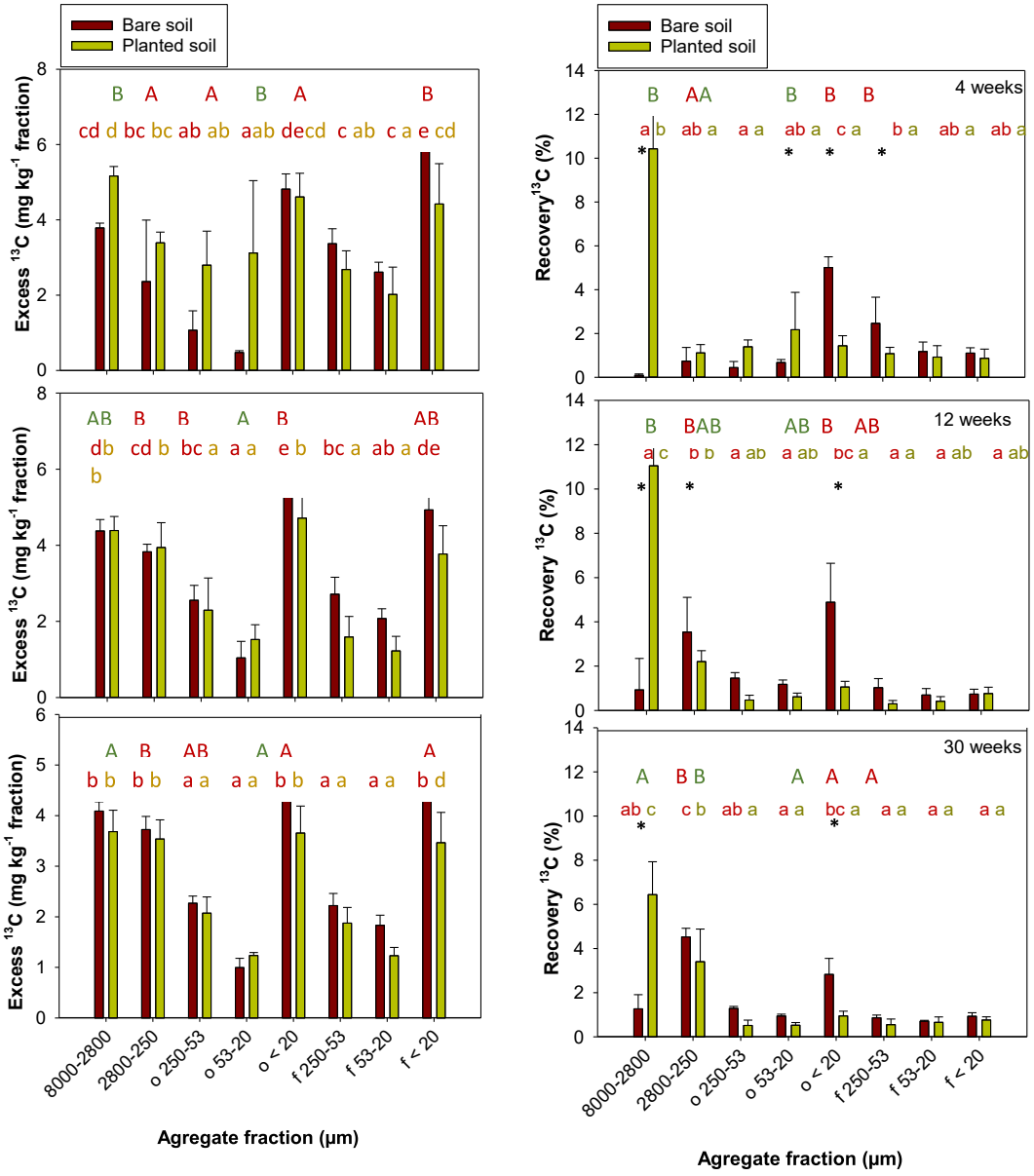

Fig. 1. Excess EPS-derived ^{13}C (left) and its recovery relative to the added amount (right) in different soil aggregate fractions 4, 12, and 30 weeks after experiment start. Different lowercase letters indicate significant differences between fractions within a given treatment and sampling time. Different capital letters indicate significant differences between sampling times within a given treatment and size fraction. The asterisks indicate significant difference between treatments (*Festuca* planted vs bare soil) within a given fraction and sampling time. Comparisons where no letters or asterisks are indicated did not show a significant difference ($p > 0.05$).

before the first sampling event (Fig. 1, right). In the bare soil treatment, the EPS-derived ^{13}C remained particularly allocated to the o <20 μm fraction, and partly shifted to smaller stable macroaggregates (2800–250 μm) with time (Fig. 1, right). In the treatment with plants, the largest amount of ^{13}C was preserved in the large stable macroaggregates (8000–2800 μm), reflecting the substantial amount of stable macroaggregates formed in this treatment (Fig. 1, right).

3.4. Fate of ^{15}N-labelled bacteria

Despite relatively high additions of labelled bacterial strains, the overall recovery of bacterial ^{15}N remained below 20 % (Table S3; Supplementary Materials). Yet, the accumulation of bacteria-derived ^{15}N correlated linearly and significantly with that of added EPS-derived ^{13}C ($R^2 = 0.72$): the relationship with EPS was particularly close in the small content range, whereas data showed more variability at >2 % excess ^{13}C (Fig. 2). As a result, and similar to ^{13}C, the largest contents of excess bacteria-derived ^{15}N were found in the <20 μm fractions, and the smallest ones in the o 53-20 μm microaggregates (Fig. 3, left). On the other hand, macroaggregates also stored a considerable amount of ^{15}N. In the bare soil treatment, the ^{15}N labels shifted from the o <20 μm fraction to the smaller stable macroaggregates (2800–250 μm) in the course of the experiment, whereas in the planted treatment particularly the large stable macroaggregates (8000–2800 μm) after 4 and 12 weeks contained most of the added bacteria-derived ^{15}N (Fig. 3, right).

The ^{15}N data also correlated linearly with qPCR gene copy numbers in the microaggregate fractions (Pearson r = 0.5, p = 0.0024). In general, the largest accumulation of bacterial material occurred in the smallest aggregate size fractions (<20 μm) (Fig. 4). This enrichment was maintained across all sampling times (Fig. 4; though partly not significant). However, we observed discrepancies for the stable macroaggregates, where ^{15}N levels were in a similar range as seen in the smallest microaggregates (Fig. 3), while gene copy numbers were much lower in the macro- than in the microaggregates (Fig. 4). Moreover, discrepancies occurred in temporal trends and total recovery. The gene copy numbers tended to decrease over time in the bare soil treatment (Fig. 4), which was less evident in the ^{15}N-data. Apparently, some ^{15}N remained in the system over the incubation period of 30 weeks upon cell lysis.

In contrast, the low recovery of bacterial ^{15}N was not reflected in the qPCR data (mean calculated recovery 100 %). Hence, these ^{15}N losses must have occurred during an early incubation phase. Although unlikely to completely explain the observed loss of ^{15}N, strains such as *Pseudomonas* may have moved from the soil bags towards the rhizosphere.

The four individual bacterial strains showed different responses in the system (significant strain × size fraction and strain × time interaction). *Gordonia* and *Methylocystis* were unevenly distributed across the size fractions with an accumulation especially in the smallest microaggregate fraction. For *Gordonia*, this uneven distribution across fractions increased over time and especially in the absence of plant growth (interactions with treatment significant; Table S4, Supplementary Materials). Similarly, *Streptomyces* was preferentially detected in specific size fractions and responded to the treatment, while *Pseudomonas* did not show a response to any of these factors. In sum, the cells accumulated initially in the o <20 μm fraction but shifted to the f <20 μm fractions as time proceeded in the bare soil, while the reverse trend was observed in the planted trials (Fig. 4). Particularly *niche pecystis* maintained a strong aggregate-specific size distribution (Table S4, Supplementary Materials).

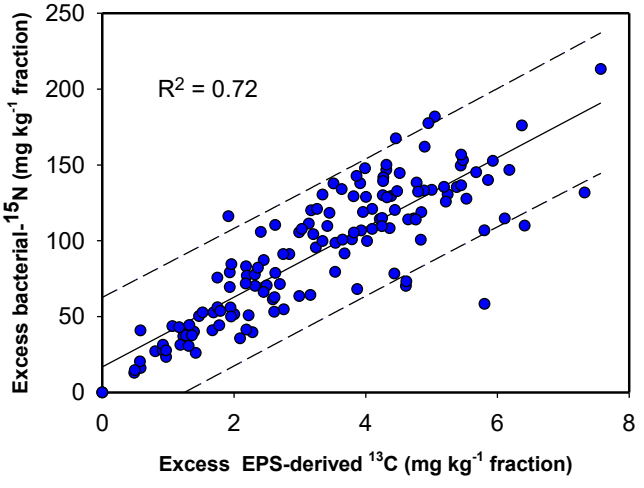

Fig. 2. Correlation between EPS-derived ^{13}C and bacteria-derived ^{15}N in different soil aggregate fractions and across different sampling times (4, 12, 30 weeks).

3.5. Fate of ^{57}Fe and ^{29}Si-labelled minerals

The added labels of ^{57}Fe and ^{29}Si were recovered with 73–96 % and 124–170 %, respectively; Table S3, Supplementary Materials). At the first sampling, both the labelled goethite and montmorillonite were distributed relatively homogeneously across the different aggregate fractions. For Fe, the presence of plants hardly affected the excess ^{57}Fe distribution, except that only after 30 weeks there were smaller ^{57}Fe signals in the o 53-20 μm fraction of the plant treatment than in the bare soil treatment (Fig. 5, left). However, the distribution across size fractions changed with time. After 30 weeks, the ^{57}Fe signal had shifted from the micro- to the stable macroaggregate fractions, irrespective of the presence of plants (Fig. 5, left).

The distribution of ^{29}Si-labelled montmorillonite correlated with that of ^{57}Fe-labelled goethite ($R^2 = 0.46$), and, similar to the organic labels, the variability of this relationship increased with elevated label content (Fig. 6). A correlation does not imply a 1:1 relationship, as the labels were not added in similar amount; indeed, it rather indicated again a potential co-allocation of the goethite with montmorillonite (Fig. S5; Supplementary Materials). At the early stage of the experiment (four weeks), the ^{29}Si signals peaked in the <20 μm fractions, though parts of this enrichment shifted to the macroaggregates during the 30 weeks of experiment duration (Fig. 5, right). As a result, the average excess ^{29}Si tended to increase in the >250 μm fractions over time, although not significant at the p <0.05 level (Fig. 5, right).

As exemplarily shown for one sample aliquot after 4 weeks incubation, different isotope labels can occur at the same particle surface, though still in spatial separation (Fig. S5, Supplementary Materials). Hence, similarities among tracers' behaviour point to similarities in the fate of the respective particles but not necessarily to direct bondings among the different tracer labels. When considering all sampling time points and fractions, the distribution of excess goethite-derived ^{57}Fe and montmorillonite-derived ^{29}Si did not correlate with EPS-derived ^{13}C or bacteria-derived ^{15}N (R^2 <0.15; p >0.05). However, these correlations existed when separating the data by treatments and time points (Table 4; Table S5, Supplementary Materials). Hence, individual interactions existed at given size fractions, time points, and treatments and these data reflect the distinct behavior of aggregation dynamics in bare soil and planted soil. The content of EPS-derived ^{13}C and bacteria-derived ^{15}N correlated in the occluded microaggretate and small stable macroaggregate fractions, while relationships of the ^{13}C-EPS label to montmorillonite-derived ^{29}Si and goethite-derived ^{57}Fe oxides were found for free microaggregates only (Table S5; Supplementary Materials). In contrast, correlations among the inorganic labels existed for nearly all fractions and time points (Table S5; Supplementary Materials). Bacteria-derived ^{15}N did mostly not relate closely to the mineral labels in certain aggregate fractions (Table S5, top), but correlations existed when considering a given treatment (bare soil, *Festuca* planted) and sampling time (Table 4; Table S5, bottom). Unfortunately, due to the limited number of samples, we were not able to decipher all factor combinations in the correlation matrix. Nevertheless, we conclude that

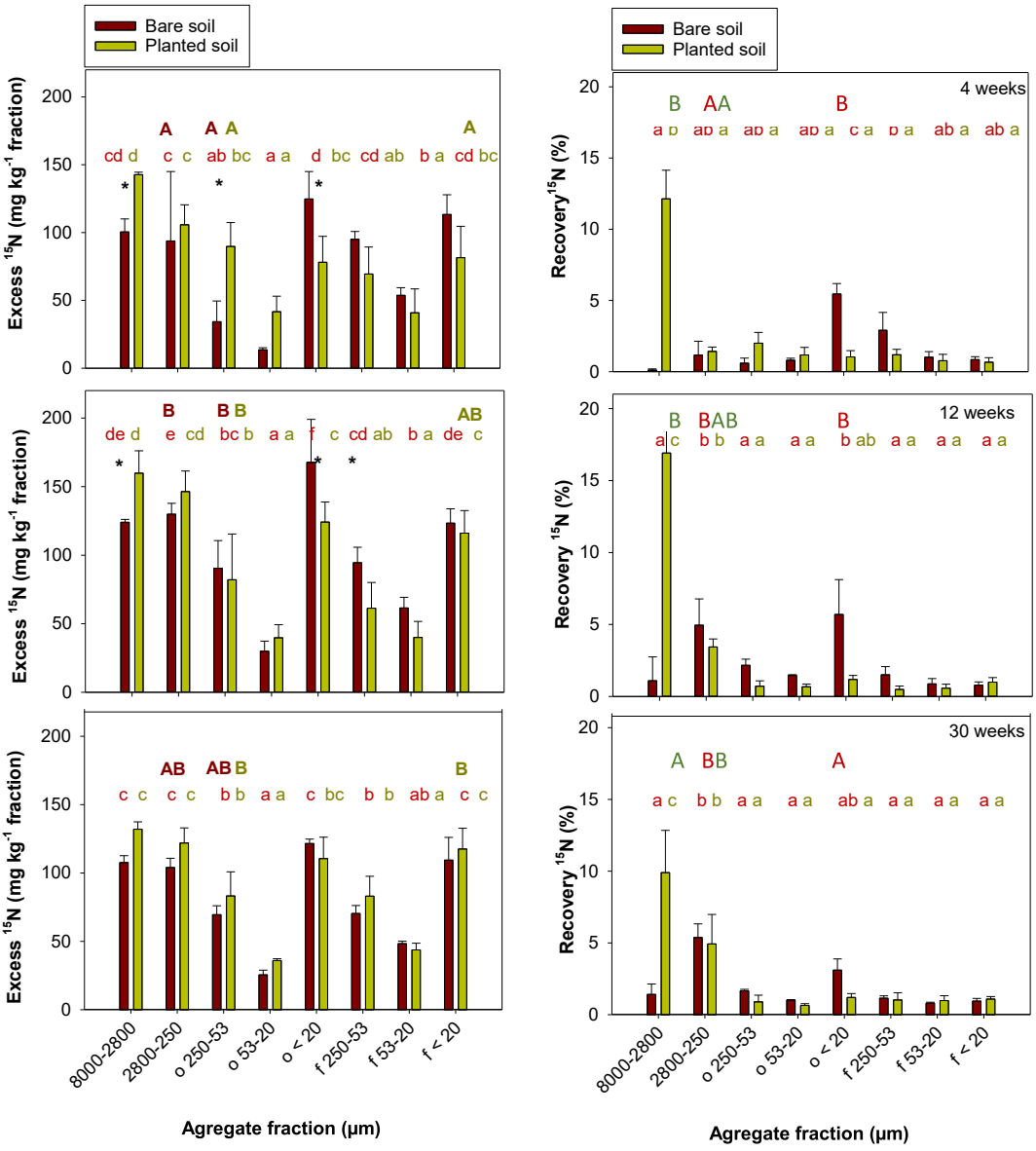

Fig. 3. Excess bacteria-derived ^{15}N (left) and its recovery relative to the added amount (right) in different soil aggregate fractions 4, 12, and 30 weeks after experiment start. Different lowercase letters indicate significant differences between fractions within a given treatment and sampling time. Different capital letters indicate significant differences between sampling dates within a given treatment and size fraction. An asterisk indicates a significant difference between treatments (*Festuca* planted vs bare soil) within a given fraction and sampling date. Comparisons where no letters or asterisks are indicated did not show a significant difference ($p > 0.05$).

EPS-derived-^{13}C and bacteria-derived-^{15}N accumulated primarily in the same size fractions where ^{29}Si-labelled montmorillonite was found, whereas correlations to ^{57}Fe-labelled goethite were weaker (Table 4; Table S5; Supplementary Materials). Hence, even if ^{57}Fe and ^{29}Si and montmorillonite largely showed similar patterns among aggregate fractions (Table S5, Supplementary Materials; Fig. 5), within these fractions, the bacteria-derived elements accumulated in closer relation to the ^{29}Si-labelled clay minerals. These correlations also appeared to become stronger with time from 4 to 12 weeks experiment duration, and even beyond for the bare soil treatments (Table 4, Table S5).

4. Discussion

4.1. Aggregate dynamics

The addition of organic gluing agents and inorganic building units leads to occlusion of free particles and microaggregates into macroaggregates (Six et al., 2004; Wagai et al., 2020; Guhra et al., 2022). In this study, we subjected all macroaggregates that did not slake after wet sieving to an ultrasonic treatment of 60 J ml^{-1} for dispersion. However, unlike earlier studies (Cambardella and Elliot, 1993; Stemmer et al., 1998; Amelung and Zech, 1999), some macroaggregates persisted this sonification (Table 2), considered here as stable macroaggregates. As it was our main aim to follow the fate of the isotope labels, we did not perform a parallel study in which no microaggregate-forming agent was added, i.e., we could not test whether the higher availability of the added organic gluing agents and inorganic microaggregate building units contributed to the stability of the detected macroaggregates against ultrasonic dispersion. However, we presume that this stabilization did not take place immediately, since the stable macroaggregates were still almost absent after 4 weeks in the bare soil treatment. Yet, this treatment contained elevated portions of occluded microaggregates (Table 2), indicating that also here macroaggregates had formed, although they did not persist during ultrasonic dispersion. Hence,

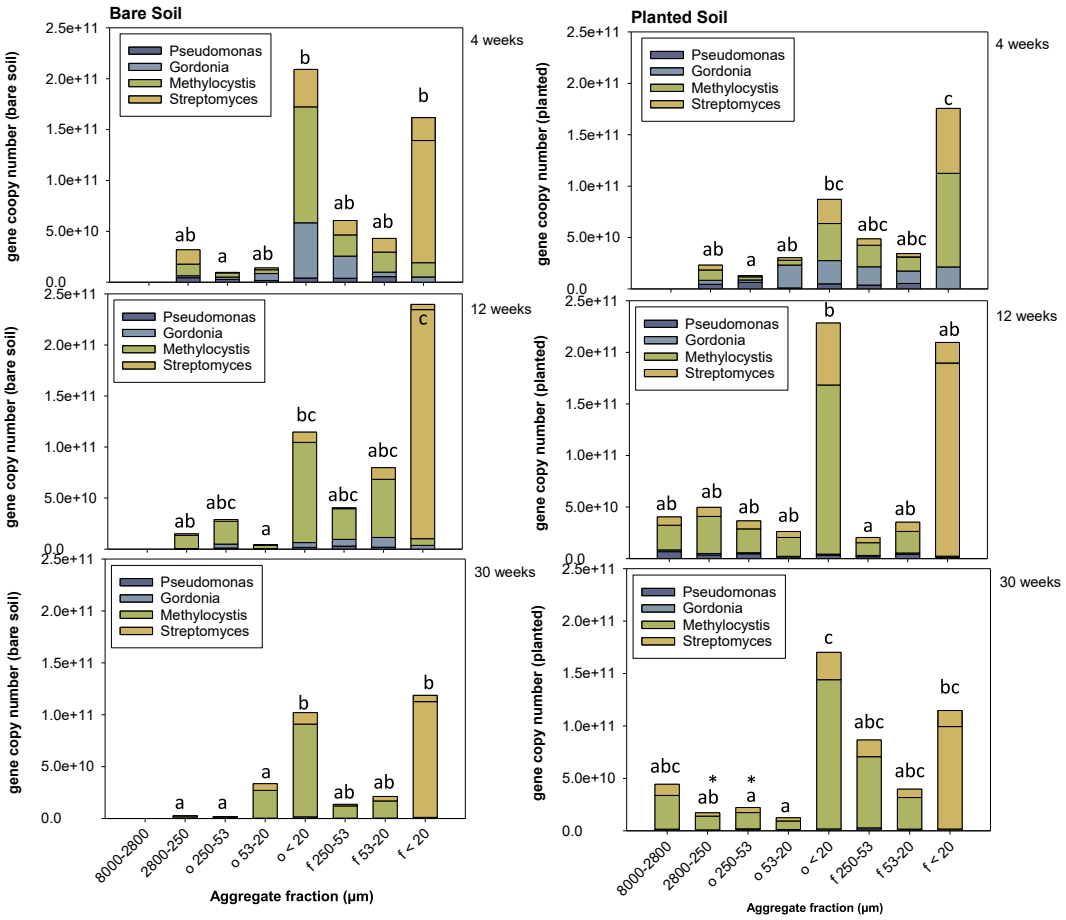

Fig. 4. Gene copy numbers of the four bacterial strains in different aggregate size fractions. Different lowercase letters indicate significant differences of total gene copy numbers between fractions within a given treatment: There were no significant differences between different sampling dates; the asterisk indicates significant differences in the planted to the bare soil, respectively (all to the $p < 0.05$ level of probability). Comparisons where no letters or asterisks are indicated did not show a significant difference.

hypothesis (1) was supported; the addition of organic gluing agents and inorganic building units (here goethite and montmorillonite) bound free particles and microaggregates into occluded ones.

The formation rates of the macroaggregates were similar to observations from adding rare earth elements to incubations; also in these experiments macroaggregates formed from sieved soil with estimated turnover rates of one month (De Gryze et al., 2005, 2006). We assume that the stable macroaggregates are still composed of microaggregate units (Oades and Waters, 1991; Six et al., 2000), but with stronger bonding to resist to ultrasonic treatment. In the planted treatment, these macroaggregates gained additional stability against ultrasonic dispersion, and their amount even exceeded that of field-fresh soil after harvest. We see this as a clear indication that the plant roots enforced aggregate stability (Six et al., 2004; Bronick and Lal, 2005), here even to an extent that microaggregates formerly occluded in ultrasonically dispersible macroaggregates were now contained in the stable macroaggregates that resisted 60 J mL^{-1} ultrasonic dispersion.

In our study, already one month of plant growth had increased total C content, and particularly the C content in the stable macroaggregates (Table 3). This finding is in line with hypothesis (2) that plants promote the formation of stable macroaggregates and occluded microaggregates by root exudation and microbial growth in the rhizosphere, whereas the effect of mere additions of EPS and bacteria on soil aggregation as in the bare soil treatment may be negligible. Particularly fine roots and fungal hyphae are known to be responsible for macroaggregate stability (Jastrow et al., 1996; Six et al., 2004). Likely, there was also an additional production of EPS and other organic gluing agents in the rhizosphere, which supported microaggregate stability (Chenu and Cosentino, 2011; Totsche et al., 2018) and possibly formed additional organic surface coatings (Amelung et al., 2002) within stable macroaggregates.

As time proceeded, stable macroaggregates also formed when plants were absent, particularly in the size range of 2000–500 µm. Hence, the presence of plant roots is not necessarily mandatory for stable macroaggregate formation. Likely, other factors such as fungal growth and physicochemical interactions of the added binding agents also induce the formation of aggregates in this size range. This macroaggregate formation, which was induced or initiated by the added macroaggregate-forming materials, however, was much less effective and particularly quantitatively less important in the long-term than macroaggregate formation and stabilization by plant roots.

The SOC contents among the fractions differed in the microaggregate fractions of different size (Table 3) in both treatments. Particularly the fine fractions <20 µm were rich in C, likely reflecting sorption of dissolved products and accumulation of microbial necromass as commonly found for these fractions (e.g., Zhang et al., 1998; Rodionov et al., 2001; Kaiser and Guggenberger, 2007). In the bare soil treatment this SOC enrichment was initially most pronounced in the occluded fraction, thus indicating to the possibility of its later involvement into ultrasonically instable macroaggregates (Six et al., 2004), and supporting earlier evidence for soil organic matter being a main agent of soil aggregation (Tisdall and Oades, 1982; Chenu and Cosentino, 2011; Totsche et al., 2018). In the planted soil this SOC enrichment in the o <20 µm fraction was not evident, suggesting that specific root-derived compounds like mucilage or microbial conversion products in the rhizosphere like

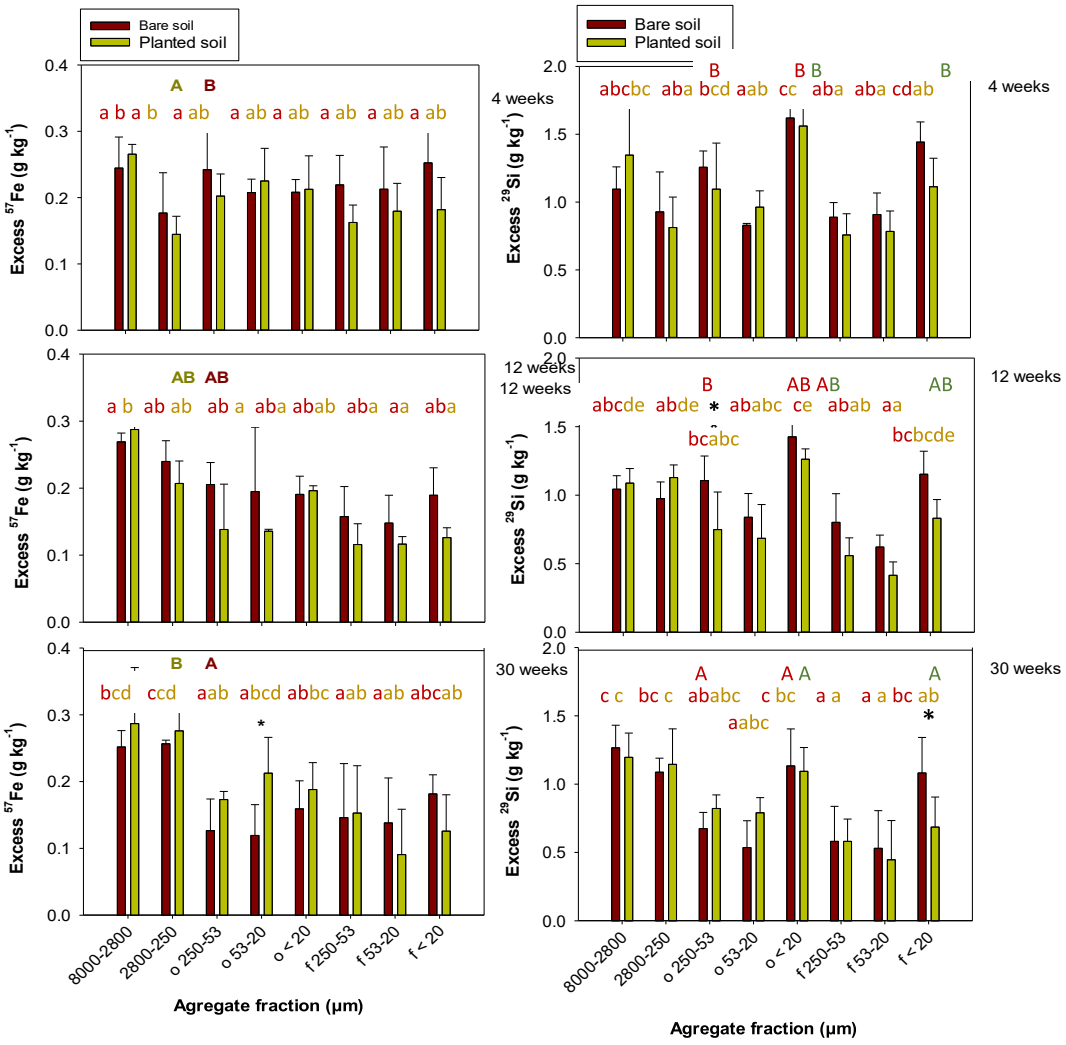

Fig. 5. Excess ^{57}Fe-goethite (left) and ^{29}Si-montmorillonite (right) in different soil aggregate fractions 4, 12, and 30 weeks after experiment start. Different lowercase letters indicate significant differences between fractions within a given treatment and sampling date. Different capital letters indicate significant differences between sampling dates within a given treatment and size fraction. An asterisk indicates a significant difference between treatments (*Festuca* planted vs bare soil) within a given fraction and sampling date. Lacking letters point to lacking statistical differences in all instances.

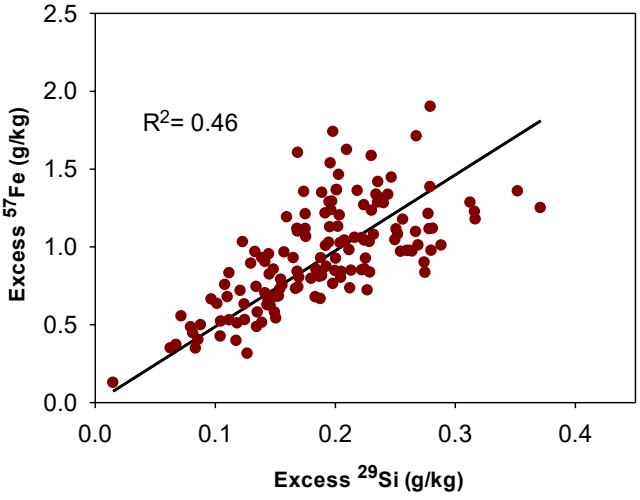

Fig. 6. Correlation between ^{57}Fe-labelled goethite and ^{29}Si-labelled montmorillonite in different soil aggregate fractions and across different sampling times (4, 12, 30 weeks).

Table 4
Linear correlation coefficients between excess of EPS-derived ^{13}C or bacteria-derived ^{15}N and excess of montmorillonite-derived ^{29}Si and goethite-derived ^{57}Fe for the different sampling times ($p < 0.05$).

Pearson r	Weeks (bare soil)			Weeks (planted soil)		
	4	12	30	4	12	30
Excess ^{13}C vs excess ^{29}Si	0.65	0.82	0.94	0.81	0.94	0.76
Excess ^{13}C vs excess ^{57}Fe	*n.s*	*n.s*	0.65	*n.s.*	0.75	*n.s.*
Excess ^{15}N vs excess ^{29}Si	*n.s*	0.79	0.92	*n.s*	0.88	0.69
Excess ^{15}N vs excess ^{57}Fe	*n.s*	*n.s*	0.67	*n.s*	0.83	*n.s*

n.s. = not significant at the $p < 0.05$ level of probability; EPS = extracellular polymeric substances.

additional EPS promoted microaggregation (Czarnes et al., 2008).

In general, variations in SOC contents within the different aggregate fractions may be due to the preferential involvement of SOC-rich microaggregates into the formation of stable macroaggregates that left SOC-poorer microaggregates behind (Six et al., 2000; Zhou et al., 2020). In addition, different SOC enrichment in different microaggregate size fractions may reflect a patchy distribution of SOM at mineral microaggregate surfaces (Moedl et al., 2007; Wagai et al., 2009; Schweizer et al., 2021), as well as different contributions of remaining primary

particles to selected microaggregate fractions (Krause et al., 2018). Particularly in the bare soil the C accrual in the stable macroaggregates after 12 weeks hardly went along with elevated C concentrations in this fraction (Table 3), possibly indicating that also other elements beside bulk C may be involved in the stabilization of aggegates in this size fraction.

Elevated Si contents in larger microaggregate fractions (Table S2, Supplementary Materials) suggest that at least some primary particles were present in the fractions, partcularly in the o 53-20 μm fraction that was enriched in Si and depleted in Fe and SOC (Table 3, Table S2, Supplementary Materials). The magnitude of the Si or Fe contents was similar among fractions, since larger aggregate units were composed of smaller ones. However, these contents changed with time and, incidentally, also treatment. With plants, not only the SOC-rich, but also the Fe-rich free microaggregates formed macroaggregates. Iron oxides contribute to organo-mineral complexation and, in addition to that, to the formation of small microaggregates (Asano et al., 2018; Totsche et al., 2018; Krause et al., 2020), which then also bind preferably to macroaggregates (which either disintegrated here to occluded microaggregates or remained stable upon ultrasonic dispersion; Table 2). The free microaggregates poor in Fe were left behind after 30 weeks of experiment duration (Table S2, Supplementary Materials). This process was promoted by plants, resulting in larger Fe contents in the occluded microaggregate fractions than in the bare soil treatment (see asterisks in Table S2, Supplementary Materials). There was possibly a feedback loop with Fe oxides binding firmly to clay minerals (Ferreiro et al., 1995; Dultz et al., 2019) and organic matter (Kaiser and Guggenberger, 2007; Guhra et al., 2019), and with the latter promoting the formation of macroaggregates, also Fe-rich microaggregates were mainly enriched in the macroaggregates. The continuous decline in Si contents likely reflected that the process of macroaggregate formation incidentally co-involved primary particles. However, only the additional stable isotope labelling allowed to follow the fate of the added microaggregate forming materials.

4.2. *Fate of isotopically labelled aggregation agents*

Extracellular polymeric substances and EPS-borne biomolecules are known as effective gluing agents for microaggregate-forming particles (Rodionov et al., 2001; Kleber et al., 2007; Totsche et al., 2018). Our data support the findings of Oades and Waters (1991) and subsequent research (e.g., Rodionov et al., 2001; Murugan et al., 2019) that particularly aggregates <20 μm were enriched with EPS materials. The EPS-derived ^{13}C was also found in silt-sized particles and aggregates <53 μm (Geoghegan and Brian, 1948; Virto et al., 2008; Fig. 1), though in smaller contents due to additional presence of primary particles (see above). Hence, this part of hypothesis 3, stating that the EPS gluing agents and bacteria bind rapidly to smaller microaggregates, was supported. For truly assessing label enrichments in relation to primary particles in microaggregates, it would have been necessary to perform an additional density fractionation (Moni et al., 2012; Krause et al., 2018), which was disregarded because of limited sample amounts.

Generally, all fractions contained EPS-derived ^{13}C, i.e., surfaces in all aggregate size classes were prone to bind EPS, irrespective of their size. With advancing aggregation, and also in line with hypothesis 3, the ^{13}C also occurred in the occluded microaggregate fractions and ultrasonically stable macroaggregates (Fig. 1). On the one hand the EPS-derived ^{13}C supports some binding of small particles as in the bare soil treatment. On the other hand, in the planted treatment this effect was inferior due to larger amounts of C added via the roots (approximately 2 g kg^{-1} soil (Table 2S; Supplementary Materials) relative to 1.22 g EPS added kg^{-1} soil (Table 1) with a C content of likely around 40 %, similar to glucose) than that added with EPS (and bacteria) alone.

Overall low EPS-derived ^{13}C recoveries suggest rapid decomposition of EPS (Fig. 1, right). A large amount of the ^{13}C-EPS was possibly lost prior to the formation of stable macroaggregates. In addition, also subsequent ^{13}C losses occurred from all fractions <250 μm, thus demonstrating that despite the strong gluing potential, there was no complete stabilization of the ^{13}C label in soil. Intriguingly, the majority of EPS-derived ^{13}C was preserved in stable macroaggregates, due to their slow turnover rates (Puget et al., 2000; Segoli et al., 2013), and likely persisted either in the intra-aggregate pore space, at the surfaces of microaggregates and particles forming these stable macroaggregates, or both.

Higher recoveries of EPS-derived ^{13}C were found in the planted treatment than in the bare soil (Fig. 1). This reflects a so-called conserving (negative priming) effect as reported earlier for straw additions (Kuzyakov et al., 2000; Wu et al., 2019b). The continued input of labile, plant-derived C renders the remaining adsorbed EPS less attractive to microbes than in the bare soil treatment. In addition, the lower amount and stability of macroaggregates in the bare soil treatment reshifted its EPS-derived ^{13}C to the occluded fractions (Fig. 1, right). Again, this points to the stabilizing effects from plant roots beyond the direct glueing of minerals via EPS.

Even though the added ^{13}C and ^{15}N stemmed from different microbial sources, there was a close correlation between EPS-derived ^{13}C and bacteria-derived ^{15}N (Fig. 2). The similar distribution pattern of the ^{15}N-labelled bacteria among fractions and for the EPS-derived ^{13}C (Figs. 1, 2) suggests that both elements likely went through the same type of biomass pool, possibly including rapid incorporation of ^{13}C-labelled EPS and bacterial necromass into microbial cells. Only at a threshold exceeding 2 % excess ^{13}C did the correlation to ^{15}N weaken (Fig. 2). The majority of bacteria was, however, likely co-preserved with EPS-derived ^{13}C in the respective macro- and microaggregates.

Remarkably, ^{15}N accumulated in larger amounts in the stable macroaggregate fraction than that observed for the DNA of the bacterial model strains. This discrepancy may point to differences in microbial biomass turnover and growth or relocation of N-substrates in dependence of soil aggregate size fraction and deserves further attention in future studies. In contrast, and in line with hypothesis 3, the <20 μm fractions consistently provided a main location of high gene copy numbers (Fig. 4), excess bacteria-^{15}N (Fig. 3), and excess EPS-derived ^{13}C (Fig. 1).

The individual bacterial strains behaved differently in the aggregate fractions over time (Fig. 4), reflecting differences in cell structure, ecological niche preference and turnover. *Pseudomonas protegens* strain CHA0 is a well-known colonizer of habitats rich in organic substrates such as the rhizosphere (Troxler et al., 2012). Thus, we expected a response to the presence of plants. However, *Pseudomonas* did not respond significantly to any of the factors; there was only a trend towards better survival in the presence of plants. The combination of the soil used here along with *Festuca* as model plant (both known to be relevant for a successful establishment of *Pseudomonas* (Meyer et al., 2010)), was apparently not suitable to support strong proliferation. Most of the cells vanished instead or turned into a dormant state (Troxler et al., 2012), therewith becoming largely unresponsive to soil aggregation processes. Likewise, the actinomycete *Gordonia* did not survive well, especially in the absence of plants. Members of this genus may occupy diverse ecological niches and degrade a variability of carbon compounds (Sowani et al., 2018), but apparently competition against the other strains and the endogenous soil microbiota was weaker and half-time shorter so that it also largely dissipated as time proceeded, especially from the larger aggregate fractions (Fig. 4). In contrast, the actinomycete *Streptomyces viridosporus* maintained a more stable population across all aggregate size fractions, not only in the presence but also in the absence of plants (Fig. 4). Due to its filamentous growth and capability to grow on recalcitrant carbon compounds, it is probably less dependent on input of fresh carbon and more independent of aggregate size (Kämpfer, 2006). Maintenance of *Metylocystis* was best in this experiment. It may have better survived compared with the other strains due to its very good adaptation to oligotrophic conditions and independence of organic carbon, by forming cysts, and/or it may have had

less predators (Knief and Dunfield, 2005, Murase and Frenzel, 2008). Its predominant accumulation in the smallest aggregate size fraction points towards a minor role for the formation of larger aggregate structures.

Intriguingly, and opposing hypothesis 3, such a preference of the gene copy numbers to small size fractions was only initially (montmorillonite) or not at all (goethite) observed for the mineral isotope label excess. Close correlations between the ^{13}C and ^{15}N labels were restrained to the occluded fractions, likely reflecting the dominant role of the biological materials in holding them together to macroaggregates (Tisdall and Oades, 1982; Totsche et al., 2018), while initial attachments of the organic labels to the mineral tracers dominated in the free macroaggregates. The latter provide the reactive surfaces most likely to be met when the experiment started.

In principle, the EPS-derived ^{13}C as well as bacteria-derived ^{15}N may firmly attach to Fe oxides and clay minerals. Correlations of these organic labels were closer to the added ^{29}Si (Table 4), possibly because clay minerals such as montmorillonite allow bacteria well to attach (Chenu and Stotzky, 2002). And since we added less goethite than montmorillonite (Table 1), similar to the soils containing usually less oxides than clay minerals, we suggest that the closer correlations to the latter might merely reflect the higher probability of organic substances coming into contact with clay mineral surfaces.

Unlike for the biological materials, an excess of the respective mineral isotope labels occurred at similar magnitude in all aggregate fractions (Fig. 5), with close correlation between the two labels (Fig. 6). We do not assume that the majority of added ^{57}Fe-goethite was directly bound to ^{29}Si-montmorillonite. The minerals were added in a dry state, not in intimate contact, and thus likely spatially separated at microscale when compared with the large volume of <250 μm sieved soil (Table 1; see also Fig. S5, Supplementary Materials). Hence, the probability that these otherwise immobile particles met in the soil is relatively low. Nevertheless, the added labelled Fe oxide and clay mineral showed a strongly contrasting behaviour during the incubation experiment compared with the organic materials added as either ^{13}C-EPS or ^{15}N-labelled cell biomass. The organic agents were mainly recovered in the macroaggregates but partly dissipated as time and aggregation proceeded. In contrast, the mineral labels increasingly shifted into the macroaggregates.

Few if any stable macroaggregates had formed in the bare soil treatment after four weeks (Table 2). Hence, also isotope labelling confirms that the presence of these minerals, whether as nucleus or associated with other minerals, is not sufficient to stabilize macroaggregates against ultrasonic dispersion – this was mainly due to the presence of plant roots by enmeshment and the effect of their rhizodeposits.

Within the microaggregates, bacterial ^{15}N and EPS-derived ^{13}C peaked in the fine fractions. This preferred binding to small aggregate fractions (hypothesis 3) was initially also observed for the ^{29}Si-montmorillonite, but it was not significant for the added goethite. As time proceeded, the enrichment of ^{57}Fe-goethite, however, shifted from the micro- to the macro-sized fractions (Fig. 5, left), and so did the ^{29}Si-montmorillonite peaks with preferred losses from the <20 μm fractions (Fig. 5, right; Table S3, Supplementary Materials). Hence, we could support hypothesis 4 that inorganic building units shift to larger particles with time, even to ultrasonically stable macroaggregates. Considering that the organic amendments in the substrate promoted the initial aggregation process, but that both the ^{13}C and ^{15}N labels were lost with time, it seems reasonable to conclude that the added minerals, goethite and montmorillonite increasingly support aggregation in the long-term. This includes the option that organic gluing agents may be replaced by others to support reaggregation, at least in the planted treatments. However, the action of dissipating organic binding agents thus leads to a much shorter cycles of aggregation, disaggregation and reaggregation than that of inorganic building units.

In line with these arguments, correlations between excess organic and inorganic isotope label concentrations changed with time: they were significant mainly after 12 weeks in the planted soil but after 30 weeks in the bare soil (Table 4), likely reflecting the slower turnover of the organic gluing agents in the bare soil trials. Disentangling individual correlations was difficult due to limited sample size; however, when grouped to aggregate fractions the analyses confirmed that organic and inorganic Fe contributions to aggregation processes were time and aggregate size-specific. Close correlations between excess ^{13}C and ^{15}N were mainly found for the occluded fractions, highlighting the role of microbial products and resynthesis for microaggregate stability (Table S5, Supplementary Materials). In contrast, intimite relations of the organic to the inorganic labels existed only for the free microaggregates but not for the occluded ones. With time, correlations with excess ^{13}C were partly significant already from the beginning, while those involving mineral fractions only developed with time, with relationships between ^{29}Si and ^{57}Fe being most pronounced towards the end of the experiment, respectively (Table S5, Supplementary Materials), reflecting that inorganic components organize in aggregates at more advanced stages of aggregate dynamics compared with organic matter.

The overall findings have general implications for the formation and turnover of aggregates in soils. The organic gluing agents were more important than their mineral counterparts for intiating macroaggregate formation. Only the presence of plant roots, however, stabilized the macroaggregates against 60 J mL^{-1} ultrasonic dispersion. The added Fe oxides, as well as clay minerals, in contrast, acted rather similar to the mineral phase already present in the soil. As there was no preference for specific size fractions they took part in all formation processes to a similar extent, including those induced by the amendment of EPS, bacteria, or through the presence of plant roots. However, while the labile organic materials degraded, the added minerals continued to stabilize the aggregates as indicated by increasing shifts to the occluded and stable aggregate fractions (Fig. 7). Hence, there appears to be a temporal sequence of aggregate formation, with individual organic substrates initializing this process and determining the degree of aggregation, and with minerals stabilizing this process in the longer-term. However, only due to the superposition of processes and organic inputs related to root growth are aggregate bondings finally strengthened to resist moderate ultrasonic dispersion (Fig. 7).

5. Conclusions

Multiple isotope-labelled organic and inorganic microaggregate-forming materials were recovered in both occluded microaggregate fractions as well as in stable macroaggregates resisting 60 J mL^{-1} ultrasonic dispersion. The build-up of macroaggregates occurred at a timescale of weeks. Without plant presence, only a few stable macroaggregates formed slowly, mainly in the size range of 2000–500 μm, i.e., the size range of binding agents alone was too small to initiate rapid macroaggregation. With *Festuca* growing, the formation of stable macroaggregates primarily occurred in the size range of 8000–2800 μm, and also contained occluded isotope-labelled microaggregates. This process intensified over time, pointing to positive feedback of organic and inorganic microaggregate forming agents and a mediation of stable macroaggregate formation by plants and fungi.

Although the ^{13}C and ^{15}N labels were added in different materials (EPS versus bacteria), their distribution and binding in different aggregate size classes were strongly correlated, particularly in the occluded fractions (Table S5, Supplementary Materials). This indicates that they undergo the same processes of binding and stabilization within aggregates, most probably controlled by rapid microbial decomposition and resynthesis during aggregate formation.

We propose a chronological sequence of aggregate formation, which superimposes the spatial aggregate hierarchy concept as deduced by Oades and Waters (1991). Organic gluing agents derived from microbes are needed to initiate the aggregation process. Mineral microaggregate-forming materials like Fe oxides and clay minerals take part in all these

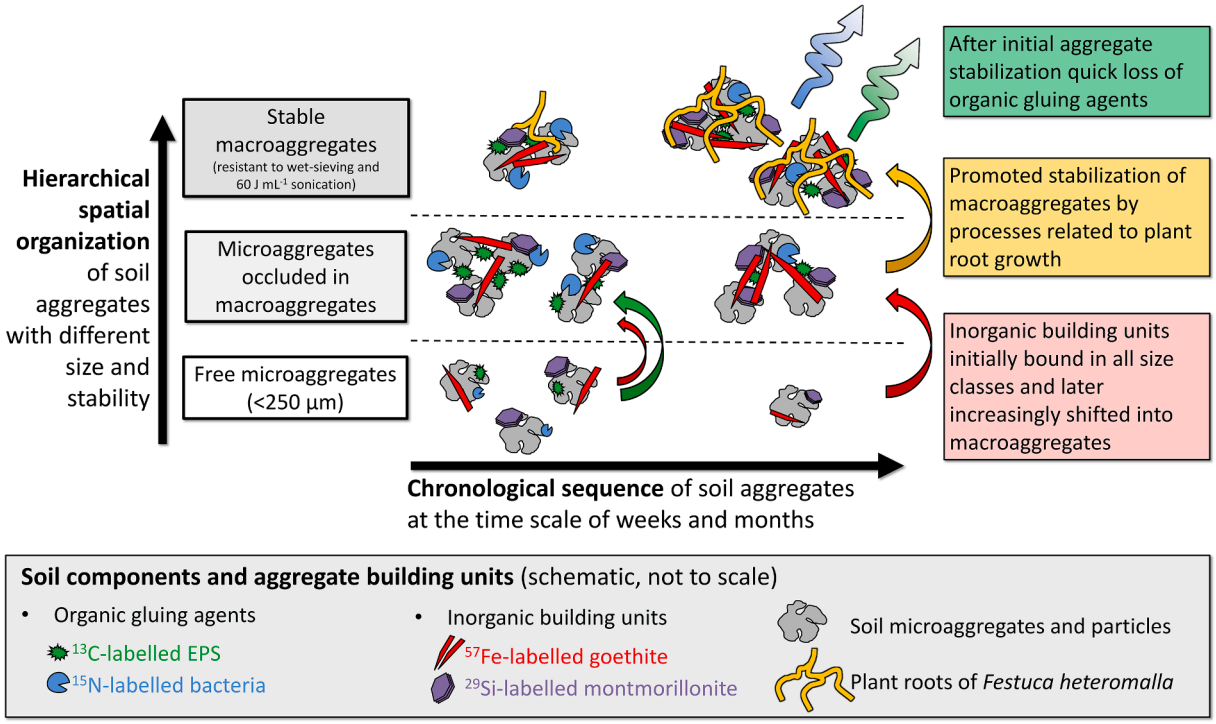

Fig. 7. Conceptual schema of the proposed process sequence of soil aggregate formation as disentangled through multiple isotopic labelling. The concerted action of organic gluing agents and inorganic building units led to a chronological sequence, which impacted the spatial organization of microaggregates and macroaggregates.

processes in all aggregate size fractions, initially to similar extent, but as time proceeds the minerals shift to the macroaggregate fractions and therewith contribute to maintaining and stabilizing their properties in the longer-term. However, only with plant roots presence can the macroaggregates be stabilized efficiently against ultrasonic dispersion. This has major implications for the aggregation, aggregate turnover and ageing in soils with respect to intensively rooted and less rooted parts, e.g., topsoil versus subsoil. Testing these scenarios under field conditions now warrants further attention.

Declaration of Competing Interest

The authors declare that they have no known competing financial interests or personal relationships that could have appeared to influence the work reported in this paper.

Data availability

All relevant data are inlcuded in the Supplementary materials

Acknowledgements

We thank Dr. Sneha Narvekar for help in the laboratory, and the German Science Foundation for funding (DFG FOR2179). The NaOH fusion digestion and ICP-OES measurements by Nadine Wettengl, ZEA-3 Forschungszentrum Juelich, and the support of Fe and Si isotope ratio measurements by Ulrike Seeling, ZEA-3 Forschungszentrum Juelich, are gratefully acknowledged.

Appendix A. Supplementary data

Supplementary data to this article can be found online at https://doi.org/10.1016/j.geoderma.2022.116226.

References

Amelung, W., Zech, W., 1999. Minimisation of organic matter disruption during particle-size fractionation of grassland epipedons. Geoderma 92, 73–85. https://doi.org/10.1016/S0016-7061(99)00023-3.

Amelung, W., Kaiser, K., Kammerer, G., Sauer, G., 2002. Organic carbon at soil particle surfaces – evidence from x-ray photoelectron spectroscopy and surface abrasion. Soil Sci. Soc. Am. J. 66, 1526–1530. https://doi.org/10.2136/sssaj2002.1526.

Angst, G., Mueller, K.E., Nierop, K.G.J., Simpson, M.J., 2021. Plant- or microbial-derived? A review on the molecular composition of stabilized soil organic matter. Soil Biol. Biochem. 156, art. no. 108189; 10.1016/j.soilbio.2021.108189.

Asano, M., Wagai, R., Yamaguchi, N., Takeichi, Y., Maeda, M., Suga, H., Takahashi, Y., 2018. In search of a binding agent: nano-scale evidence of preferential carbon associations with poorly-crystalline mineral phases in physically-stable, clay-sized aggregates. Soil Syst. 2, 32. https://doi.org/10.3390/soilsystems2020032.

Biesgen, D., Frindte, K., Maarasstawi, S., Knief, C., 2020. Clay content modulates differences in bacterial community structure in soil aggregates of different size. Geoderma 376, 114544. https://doi.org/10.1016/j.geoderma.2020.114544.

Bronick, C.J., Lal, R., 2005. Soil structure and management. Geoderma 124, 3–22. https://doi.org/10.1016/j.geoderma.2004.03.005.

Bucka, F.B., Kölbl, A., Uteau, D., Peth, S., Kögel-Knabner, I., 2019. Organic matter input determines structure development and aggregate formation in artificial soils. Geoderma 354, 113881. https://doi.org/10.1016/j.geoderma.2019.113881.

Bucka, F.B., Felde, V.J.M.N.L., Peth, S., Kögel-Knabner, I., 2021. Disentangling the effects of OM quality and soil texture on microbially mediated structure formation in artificial model soils. Geoderma 403, 115213. https://doi.org/10.1016/j.geoderma.2021.115213.

Buyanovsky, G.A., Aslam, M., Wagner, G.H., 1994. Carbon turnover in soil physical fractions. Soil Sci. Soc. Am. J. 58, 1167–1173. https://doi.org/10.2136/sssaj1994.03615995005800040023x.

Cambardella, C.A., Elliot, E.T., 1993. Methods for physical fractionation and characterisation of soil organic matter fractions. Geoderma 56, 449–457. https://doi.org/10.1016/0016-7061(93)90126-6.

Cambier, P., 1986. Infrared study of goethites of varying crystallinity and particle size: II: Crystallographic and morphological changes in series of synthetic goethites. Clay Min. 21, 201–210. https://doi.org/10.1180/claymin.1986.021.2.09.

Chenu, C., Cosentino, D.J., 2011. Microbial regulation of soil structure dynamics. In: Ritz, K., Young, I. (Eds.), The Architechture and Biology of Soils: Life in Inner Space. CAB International, Wallingford, pp. 37–70.

Chenu, C., Plante, A.F., 2006. Clay-sized organo-mineral complexes in a cultivation chronosequence: revisiting the concept of the 'primary organo-mineral complex'. Eur. J. Soil Sci. 57, 596–607. https://doi.org/10.1111/j.1365-2389.2006.00834.x.

Chenu, C., Stotzky, G., 2002. Interactions between microorganisms and soil particles: An overview. In: Huang, P.M., Bollag, J.M., Senesi, N. (Eds.), Interactions Between Soil Particles and Microorganisms. Wiley and Sons, New York, pp. 3–40.

Cheshire, M.V., 1985. Carbohydrates in relation to soil fertility. In: Vaughan, D., Malcolm, R.E. (Eds.), Soil Organic Matter and Biological Activity. The Netherlands, Springer, Dordrecht, pp. 263–288.
Czarnes, S., Hallett, P.D., Bengough, A.G., Young, I.M., 2008. Root-and microbial-derived mucilages affect soil structure and water transport. Eur. J. Soil Sci. 51 (3), 435–443. https://doi.org/10.1046/j.1365-2389.2000.00327.x.
De Gryze, S., Six, J., Brits, C., Merckx, R., 2005. A quantification of short-term macroaggregate dynamics: influences of wheat residue input and texture. Soil Biol. Biochem. 37, 55–66. https://doi.org/10.1016/j.soilbio.2004.07.024.
Decho, A.W., Moriarty, D.J.W., 1990. Bacterial exopolymer utilization by a harpacticoid copepod - a methodology and results. Limnol. Oceanogr. 35, 1039–1049. https://doi.org/10.4319/lo.1990.35.5.1039.
DeGryze, S., Six, J., Merckx, R., 2006. Quantifying water-stable soil aggregate turnover and its implication for soil organic matter dynamics in a model study. Eur. J. Soil Sci. 57, 693–707. https://doi.org/10.1111/j.1365-2389.2005.00760.x.
Dultz, S., Woche, S.K., Mikutta, R., Schrapel, M., Guggenberger, G., 2019. Size and charge constraints in microaggregation: model experiments with mineral particle-size fractions. Appl. Clay Sci. 170, 29–40. https://doi.org/10.1016/j.clay.2019.01.002.
Ferreiro, E.A., Helmy, A.K., de Bussetti, S.G., 1995. Interaction of Fe-Oxyhydroxide colloidal particles with montmorillonite. Clay Min. 30, 195–200. https://doi.org/10.1180/claymin.1995.030.3.03.
Foster, R., 1988. Microenvironments of soil microorganisms. Biol. Fert. Soils 6, 189–203. https://doi.org/10.1007/BF00260816.
Frindte, K., Lehndorff, E., Vlaminck, S., Werner, K., Kehl, M., Khormali, F., Knief, C., 2020. Evidence for signatures of ancient microbial life in paleosols. Sci. Rep. 10, 16830. https://doi.org/10.1038/s41598-020-73938-9.
Geoghegan, M., Brian, R., 1948. Aggregate formation in soil. 1. Influence of some bacterial polysaccharides on the binding of soil particles. Biochem. J. 43, 5.
Guggenberger, G., Elliott, E.T., Frey, S.D., Six, J., Paustian, K., 1999. Microbial contributions to the aggregation of a cultivated grassland soil amended with starch. Soil Biol. Biochem. 31, 407–419. https://doi.org/10.1016/S0038-0717(98)00143-6.
Guhra, T., Ritschel, T., Totsche, K.U., 2019. Formation of mineral-mineral and organo-mineral composite building units from microaggregate-forming materials including microbially produced extracellular polymeric substances. Eur. J. Soil Sci. 70, 604–615. https://doi.org/10.1111/ejss.12774.
Guhra, T., Stolze, K., Totsche, K.U., 2022. Pathways of biogenically excreted organic matter into soil aggregates. Soil Biol. Biochem. 164, 108483 https://doi.org/10.1016/j.soilbio.2021.108483.
Gulde, S., Chung, H., Amelung, W., Chang, C., Six, J., 2008. Soil carbon saturation controls labile and stable carbon pool dynamics. Soil Sci. Soc. Am. J. 72, 605–612. https://doi.org/10.2136/sssaj2007.0251.
Jaber, M., Komarneni, S., Zhou, C.-H., 2012. Synthesis of clay minerals. In: Bergaya, F., Lagaly, G. (Eds.), Handbook of Clay Science, 2nd Ed. Elsevier, Amsterdam, pp. 223–241.
Jacquemot, P., Viennet, J.-C., Bernard, S., Le Guillou, C., Rigaud, B., Georgelin, T., Jaber, M., 2019. The degradation of organic compounds impacts the crystallization of clay minerals and vice versa. Sci. Rep. 9, 20251. https://doi.org/10.1038/s41598-019-56756-6.
Jastrow, J.D., 1996. Soil aggregate formation and the accrual of particulate and mineralassociated organic matter. Soil Biol. Biochem. 28, 665–676. https://doi.org/10.1016/0038-0717(95)00159-X.
Jastrow, J.D., Miller, R.M., Boutton, T.W., 1996. Carbon dynamics of aggregate-associated organic matter estimated by carbon-13 natural abundance. Soil Sci. Soc. Am. J. 60 (3), 801–807. https://doi.org/10.2136/sssaj1996.03615995006000030017x.
John, B., Yamashita, T., Ludwig, B., Flessa, H., 2005. Storage of organic carbon in aggregate and density fractions of silty soils under different types of land use. Geoderma 128, 63–79. https://doi.org/10.1016/j.geoderma.2004.12.013.
Kaiser, M., Berhe, A.A., 2014. How does sonication affect the mineral and organic constituents of soil aggregates?—A review. J. Plant Nutr. Soil Sci. 177 (4), 479–495. https://doi.org/10.1002/JPLN.201300339.
Kaiser, K., Guggenberger, G., 2007. Sorptive stabilization of organic matter by microporous goethite: sorption into small pores vs. surface complexation. Eur. J. Soil Sci. 58, 45–59. https://doi.org/10.1111/j.1365-2389.2006.00799.x.
Kämpfer,, 2006. The Family Streptomycetaceae. Part I: Taxonomy. In: The Prokaryotes 3, pp. 538–604. https://doi.org/10.1007/0-387-30743-5_22.
Kleber, M., Sollins, P., Sutton, R., 2007. A conceptual model of organo-mineral interactions in soils: self-assembly of organic molecular fragments into zonal structures on mineral surfaces. Biogeochem. 85, 9–24. https://doi.org/10.1007/s10533-007-9103-5.
Knief, C., Dunfield, P.F., 2005. Response and adaptation of different methanotrophic bacteria to low methane mixing ratios. Environm. Microbiol. 7, 1307–1317. https://doi.org/10.1111/j.1462-2920.2005.00814.x.
Kögel-Knabner, I., Amelung, W., 2021. Soil organic matter in major pedogenetic soil groups. Geoderma 384, 14785. https://doi.org/10.1016/j.geoderma.2020.114785.
Kögel-Knabner, I., Guggenberger, G., Kleber, M., Kandeler, E., Kalbitz, K., Scheu, S., Eusterhues, K., Leinweber, P., 2008. Organo-mineral associations in temperate soils: integrating biology, mineralogy and organic matter chemistry. J. Plant Nutr. Soil Sci. 171, 61–82. https://doi.org/10.1002/jpln.200700048.
Kösters, R., Preger, A., DuPreez, C.C., Amelung, W., 2013. Re-aggregation of degraded cropland soils with prolonged secondary pasture management in the South African Highveld. Geoderma 192, 173–181. https://doi.org/10.1016/j.geoderma.2012.07.011.
Krause, L., Rodionov, A., Schweizer, S.A., Siebers, N., Lehndorff, E., Klumpp, E., Amelung, W., 2018. Microaggregate stability and storage of organic carbon is affected by clay content in arable Luvisols. Soil Till. Res. 182, 123–129. https://doi.org/10.1016/j.still.2018.05.003.
Krause, L., Klumpp, E., Nofz, I., Missong, A., Amelung, W., Siebers, N., 2020. Colloidal Iron and organic carbon controls on aggregate formation and stability as affected by clay content. Geoderma 374, 114421. https://doi.org/10.1016/j.geoderma.2020.114421.
Kummer, C., Schumann, P., Stackebrandt, E., 1999. *Gordonia alkanivorans* sp. nov., isolated from tar-contaminated soil. Int. J. Syst. Bacteriol. 49, 1513–1522. https://doi.org/10.1099/00207713-49-4-1513.
Kuzyakov, Y., Blagodatskaya, E., 2015. Microbial hotspots and hot moments in soil: Concept & review. Soil Biol. Biochem. 83, 184–199. https://doi.org/10.1016/j.soilbio.2015.01.025.
Kuzyakov, Y., Friedel, J., Stahr, K., 2000. Review of mechanisms and quantification of priming effects. Soil Biol. Biochem. 32, 1485–1498. https://doi.org/10.1016/S0038-0717(00)00084-5.
Ladd, J.N., Foster, R.C., Skjemstad, J.O., 1993. Soil structure: carbon and nitrogen metabolism. Soil Struct./Soil Biota Interrelat. 401–434 https://doi.org/10.1016/B978-0-444-81490-6.50034-0.
Lehmann, J., Kinyangi, J., Solomon, D., 2007. Organic matter stabilization in soil microaggregates: implications from spatial heterogeneity of organic carbon contents and carbon forms. Biogeochem. 85, 45–57. https://doi.org/10.1007/s10533-007-9105-3.
Lehmann, J., Solomon, D., Kinyangi, J., Dathe, L., Wirick, S., Jacobsen, C., 2008. Spatial complexity of soil organic matter forms at nanometer scales. Nature Geosci. 1, 238–242. https://doi.org/10.1038/ngeo155.
Lehndorff, E., Rodionov, A., Plümer, L., Rottmann, P., Spiering, B., Dultz, S., Amelung, W., 2021. Spatial organization of soil microaggregates. Geoderma 386, 114915. https://doi.org/10.1016/j.geoderma.2020.114915.
Lenth, R., 2018. Package ''lsmeans', Version 2.30-0. https://cran.r-project.org/web/packages/lsmeans/lsmeans.pdf.
Li, Y.Y., Shao, M.A., 2006. Change of soil physical properties under long-term natural vegetation restoration in the loess plateau of China. J. Arid Environ. 64, 77–96. https://doi.org/10.1016/j.jaridenv.2005.04.005.
Liu, X., Eusterhues, K., Thieme, J., Ciobota, V., Höschen, C., Mueller, C.W., Küsel, K., Kögel-Knabner, I., Rösch, P., Popp, J., Totsche, K.U., 2013. STXM and NanoSIMS investigations on EPS fractions before and after adsorption to goethite. Environ. Sci. Technol. 47, 3158–3166. https://doi.org/10.1021/es3039505.
Lobe, I., Sandhage-Hofmann, A., Brodowski, S., du Preez, C.C., Amelung, W., 2011. Aggregate dynamics and associated soil organic matter contents as influenced by prolonged arable cropping in the South African Highveld. Geoderma 162, 251–259. https://doi.org/10.1016/j.geoderma.2011.02.001.
Meyer, J.B., Lutz, M.P., Frapolli, M., Pechy-Tarr, M., Rochat, L., Keel, C., Defago, G., Maurhofer, M., 2010. Interplay between wheat cultivars, biocontrol pseudomonads and soil. Appl. Environ. Microbiol. 76 (18), 6196–6204. https://doi.org/10.1128/AEM.00752-10.
Moedl, C., Wörmann, H., Amelung, W., 2007. Contrasting effects of different types of organic material on surface area and microaggregation of goethite. Geoderma 141, 167–173. https://doi.org/10.1016/j.geoderma.2007.05.003.
Moni, C., Derrien, D., Hatton, P.J., Zeller, B., Kleber, M., 2012. Density fractions versus size separates: does physical fractionation isolate functional soil compartments? Biogeosci. 9, 5181–5197. https://doi.org/10.5194/bg-9-5181-2012.
Murase, J., Frenzel, P., 2008. Selective grazing of methanotrophs by protozoa in a rice field soil. FEMS Microbiol. Ecol. 65 (3), 408–414. https://doi.org/10.1111/j.1574-6941.2008.00511.x.
Murugan, R., Djukic, I., Keiblinger, K., Zehetner, F., Bierbaumer, M., Zechmeister-Bolternstern, S., Joergernsen, S.G., 2019. Spatial distribution of microbial biomass and residues across soil aggregate fractions at different elevations in the Central Austrian Alps. Geoderma 339, 1–8. https://doi.org/10.1016/j.geoderma.2018.12.018.
Oades, J.M., 1988. The retention of organic matter in soils. Biogeochem. 5, 35–70. https://doi.org/10.1007/BF02180317.
Oades, J.M., Waters, A.G., 1991. Aggregate hierarchy in soils. Austr. J. Soil Res. 29, 815–828. https://doi.org/10.1071/SR9910815.
Omoike, A., Chorover, J., 2006. Adsorption to goethite of extracellular polymeric substances from Bacillus subtilis. Geochim. Cosmochim. Acta 70, 827–838. https://doi.org/10.1016/j.gca.2005.10.012.
Opfergelt, S., Delmelle, P., 2012. Silicon isotopes and continental weathering processes: Assessing controls on Si transfer to the ocean. C. R. Geosci. 344, 723–738. https://doi.org/10.1016/j.crte.2012.09.006.
Péchy-Tarr, M., Borel, N., Kupferschmied, P., Turner, V., Binggeli, O., Radovanovic, D., Maurhofer, M., Keel, C., 2013. Control and host-dependent activation of insect toxin expression in a root-associated biocontrol pseudomonad. Environm. Microbiol. 15, 736–750. https://doi.org/10.1111/1462-2920.12050.
Peng, X., Zhu, Q., Zhang, Z., Hallett, P.D., 2017. Combined turnover of carbon and soil aggregates using rare earth oxides and isotopically labelled carbon as tracers. Soil Biol. Biochem. 109, 81–94. https://doi.org/10.1016/j.soilbio.2017.02.002.
Pinheiro, J., Bates, .D, DebRoy, S., Sarkar, D., Heisterkamp, S., Van Willigen, B., Maintainer, R., 2017. Package 'nlme', Version 3.1-152. https://cran.r-project.org/web/packages/nlme/nlme.pdf.
Plante, A.F., Duke, M.J., McGill, W.B., 1999. A tracer sphere detectable by neutron activation for soil aggregation and translocation studies. Soil Sci. Soc. Am. J. 63, 1284–1290.
Pridham, T.G., Hesseltine, C.W., Benedict, R.G., 1958. A guide for the classification of streptomycetes according to selected groups – Placement of strains in morphological sections. Appl. Microbiol. 6, 52–79. https://doi.org/10.1128/am.6.1.52-79.1958.

Pronk, G.J., Heister, K., Ding, G.-C., Smalla, K., Kögel-Knabner, I., 2012. Development of biogeochemical interfaces in an artificial soil incubation experiment; aggregation and formation of organomineral associations. Geoderma 189, 585–594. https://doi.org/10.1016/j.geoderma.2012.05.020.

Puget, P., Chenu, C., Balesdent, J., 2000. Dynamics of soil organic matter associated with particle-size fractions of water-stable aggregates. Eur. J. Soil Sci. 51, 595–605. https://doi.org/10.1111/j.1365-2389.2000.00353.x.

R Core Team, 2020. R: A Language and Environment for Statistical Computing. R Foundation for Statistical Computing, Vienna, Austria. URL.

Rahman, M.T., Liu, S., Guo, Z.C., Zhang, Z.B., Peng, X.H., 2019. Impacts of residue quality and N input on aggregate turnover using the combined ^{13}C natural abundance and rare earth oxides as tracers. Soil Till. Res. 189, 110–122. https://doi.org/10.1016/j.still.2019.01.005.

Rasmussen, C., Heckman, K., Wieder, W.R., Keiluweit, M., Lawrence, C.R., Berhe, A.A., Blankinship, J.C., Crow, S.E., Druhan, J.L., Hicks-Pries, C.E., Spiotta, E.M., Plante, A. F., Schädel, C., Schimmel, J.P., Sierra, C.A., Thompson, A., Wagai, R., 2018. Beyond clay: towards an improved set of variables for predicting soil organic matter content. Biogeochemistry 137, 297–306 (2018). 10.1007/s10533-018-0424-3.

Reinhold-Hurek, B., Bunger, W., Burbano, S.F., Sabale, M., Hurek, T., 2015. Roots shaping their microbiome: global hotspots for microbial activity. Annu. Rev. Phytopathol. 53, 403–424. https://doi.org/10.1146/annurev-phyto-082712-102342.

Rhee, S.-K., Chang, J.H., Chang, Y.K., Chang, H.N., 1998. Desulfurization of dibenzothiophene and diesel oils by a newly isolated Gordona strain, CYKS1. Appl. Environm. Microbiol. 64, 2327–2331. https://doi.org/10.1128/AEM.64.6.2327-2331.1998.

Rillig, M.C., 2004. Arbuscular mycorrhizae, glomalin, and soil aggregation. Can. J. Soil Sci. 84, 355–363. https://doi.org/10.4141/S04-003.

Rodionov, A., Amelung, W., Urusevskaja, I., Zech, W., 2001. Origin of the enriched labile fraction (ELF) in Russian Chernozems with different site history. Geoderma 102, 299–315. https://doi.org/10.1016/S0016-7061(01)00038-6.

Rodionov, A., Lehndorff, E., Stremtan, C., Brand, W., Königshoven, P., Amelung, W., 2019. In-situ mapping of natural 12C/13C abundance in environmental samples using laser-ablation isotope-ratio-mass spectrometry. Anal. Chem. 91, 6225–6232. https://doi.org/10.1021/acs.analchem.9b00892.

Schielzeth, H., Dingemanse, N.J., Nakagawa, S., Westneat, D.F., Allegue, H., Teplitsky, C., Réale, D., Dochtermann, N.A., Garamszegi, L.Z., Araya-Ajoy, Y.G., 2020. Robustness of linear mixed-effects models to violations of distributional assumptions. Meth. Ecol. Evol. 11, 1141–1152. https://doi.org/10.1111/2041-210X.13434.

Schweizer, S.A., Bucka, F.B., Graf-Rosenfellner, M., Kögel-Knabner, I., 2019. Soil microaggregate size composition and organic matter distribution as affected by clay content. Geoderma 355, 113901. https://doi.org/10.1016/j.geoderma.2019.113901.

Schweizer, S.A., Mueller, C.W., Höschen, C., Ivanov, P., Kögel-Knabner, I., 2021. The role of clay content and mineral surface area for soil organic carbon storage in an arable toposequence. Biogeochem. https://doi.org/10.1007/s10533-021-00850-3.

Segoli, M., De Gryze, S., Dou, F., Lee, J., Post, W.M., Denef, K., Six, J., 2013. AggModel: A soil organic matter model with measurable pools for use in incubation studies. Ecol. Modell. 263, 1–9. https://doi.org/10.1016/j.ecolmodel.2013.04.010.

Siebers, N., Abdelrahman, H., Krause, L., Amelung, W., 2018. Bias in aggregate geometry and properties after disintegration and drying procedures. Geoderma 313, 163–171. https://doi.org/10.1016/j.geoderma.2017.10.028.

Six, J., Elliott, E.T., Paustian, K., 2000. Soil macroaggregate turnover and micro-aggregate formation: a mechanism for C sequestration under no-tillage agriculture. Soil Biol. Biochem. 32, 2099–2103. https://doi.org/10.1016/S0038-0717(00)00179-6.

Six, J., Bossuyt, H., DeGryze, S., Denef, K., 2004. A history of research on the link between (micro)aggregates, soil biota, and soil organic matter dynamics. Soil Till. Res. 79, 7–31. https://doi.org/10.1016/j.still.2004.03.008.

Sowani, H., Kulkarni, M., Zinjarde, S., 2018. An insight into the ecology, diversity and adaptations of Gordonia species. Crit. Rev. Microbiol. 44 (4), 393–413. https://doi.org/10.1080/1040841X.2017.1418286.

Staricka, J.A., Allmaras, R.R., Nelson, W.W., Larson, W.E., 1992. Soil aggregate longevity as determined by the incorporation of ceramic spheres. Soil Sci. Soc. Am. J. 56, 1591–1597. https://doi.org/10.2136/sssaj1992.03615995005600050042x.

Stemmer, M., Gerzabek, M.H., Kandeler, E., 1998. Organic matter and enzyme activity in particle-size fractions of soils obtained after low-energy sonication. Soil Biol. Biochem. 30, 9–17. https://doi.org/10.1016/S0038-0717(97)00093-X.

Stemmer, M., von Lützow, M., Kandeler, E., Pichlmayer, F., Gerzabek, M.H., 1999. The effect of maize straw placement on mineralization of C and N in soil particle size fractions. Eur. J. Soil Sci. 50, 73–86. https://doi.org/10.1046/j.1365-2389.1999.00204.x.

Tamrat, W.Z., Rose, J., Grauby, O., Doelsch, E., Levard, C., Chaurand, P., Basile-Doelsch, I., 2019. Soil organo-mineral associations formed by co-precipitation of Fe, Si and Al in presence of organic ligands. Geochim. Cosmochim. Acta 260, 15–28. https://doi.org/10.1016/j.gca.2019.05.043.

Tisdall, J.M., Oades, J.M., 1982. Organic matter and water-stable aggregates in soils. J. Soil Sci. 33, 141–163. https://doi.org/10.1111/j.1365-2389.1982.tb01755.x.

Totsche, K.U., Amelung, W., Gerzabek, M.H., Guggenberger, G., Klumpp, E., Knief, C., Lehndorff, E., Mikutta, R., Peth, S., Prechtel, A., Ray, N., Kögel-Knabner, I., 2018. Microaggregates in soils. J. Plant Nutr. Soil Sci. 181, 104–136. https://doi.org/10.1002/jpln.201600451.

Troxler, J., Svercel, M., Natsch, A., Zala, M., Keel, C., Moënne-Loccoz, Y., Défago, G., 2012. Persistence of a biocontrol Pseudomonas inoculant as high populations of culturable and non-culturable cells in 200-cm-deep soil profiles. Soil Biol. Biochem. 44, 122–129. https://doi.org/10.1016/j.soilbio.2011.09.020.

Virto, I., Barre, P., Chenu, C., 2008. Microaggregation and organic matter storage at the silt-size scale. Geoderma 146, 326–335. https://doi.org/10.1016/j.geoderma.2008.05.021.

Vogel, C., Mueller, C.W., Höschen, C., Buegger, F., Heister, K., Schulz, S., Schloter, M., Kögel-Knabner, I., 2014. Submicron structures provide preferential spots for carbon and nitrogen sequestration in soils. Nat. Commun. 5, 2947. https://doi.org/10.1038/ncomms3947.

Volder, A., Gifford, R.M., Evans, J.R., 2007. Effects of elevated atmospheric CO2, cutting frequency, and differential day/night atmospheric warming on root growth and turnover of nPhalaris swards. Glob. Change Biol. 13, 1040–1052. https://doi.org/10.1111/j.1365-2486.2007.01321.x.

Voltolini, M., Taş, N., Wang, S., Brodie, E.L., Ajo-Franklin, J.B., 2017. Quantitative characterization of soil micro-aggregates: New opportunities from sub-micron resolution synchrotron X-ray microtomography. Geoderma 305, 382–393. https://doi.org/10.1016/j.geoderma.2017.06.005.

Wagai, R., Mayer, L.M., Kitayama, K., 2009. Extent and nature of organic coverage of soil mineral surfaces assessed by a gas sorption approach. Geoderma 149, 152–160. https://doi.org/10.5194/soil-6-597-2020032.

Wang, X., Yin, L., Dijkstra, F.A., Lu, J., Wang, P., Cheng, W., 2020. Rhizosphere priming is tightly associated with root-driven aggregate turnover. Soil Biol. Biochem. 149, 107964. 10.1016/j.soilbio.2020.107964.

Watteau, F., Villemin, G., Burtin, G., Jocteur-Monrozier, L., 2006. Root impact on the stability and types of micro-aggregates in silty soil under maize. Eur. J. Soil Sci. 57, 247–257. https://doi.org/10.1111/j.1365-2389.2005.00734.x.

Watts, C., Whalley, W., Brookes, P., Devonshire, B., Whitmore, A., 2005. Biological and physical processes that mediate micro-aggregation of clays. Soil Sci. 170, 573–583. https://doi.org/10.1097/01.ss.0000178206.74040.0c.

Wu, B., Amelung, W., Xing, Y., Bol, R., Berns, A.E., 2019a. Iron cycling and isotope fractionation in terrestrial ecosystems. Earth Sci. Rev. 190, 323–352. https://doi.org/10.1016/j.earscirev.2018.12.012.

Wu, L., Zhang, W., Wei, W., He, Z., Kuzyakov, Y., Bol, R., Hu, R., 2019b. Soil organic matter priming and carbon balance after straw addition is regulated by long-term fertilization. Soil Biol. Biochem. 135, 383–391. https://doi.org/10.1016/j.soilbio.2019.06.003.

Wagai, R., Kajiura, M., and Asano, M., 2020. Iron and aluminum association with microbially processed organic matter via meso-density aggregate formation across soils: organo-metallic glue hypothesis, SOIL, 6, 597–627, 10.5194/soil-6-597-2020.

Zech, S., Dultz, S., Guggenberger, G., Prechtel, A., Ray, N., 2020. Microaggregation of goethite and illite evaluated by mechanistic modeling Appl. Clay Sci. 198, 105845 https://doi.org/10.1016/j.clay.2020.105845.

Zhang, X., Amelung, W., Yuan, Y., Zech, W., 1998. Amino sugar signature of particle-size fractions in soils of the native prairie as affected by climate. Soil Sci. 163, 220–229. https://doi.org/10.1097/00010694-199803000-00007.

Zhou, M., Liu, C., Wang, J., Meng, Q., Yuan, Y., Ma, X., Liu, X., Zhu, Y., Ding, G., Zhang, J., Zeng, X., Du, W., 2020. Soil aggregates stability and storage of soil organic carbon respond to cropping systems on Black Soils of Northeast China. Sci. Rep. 10, 265. https://doi.org/10.1038/s41598-019-57193-1.